A GENERALIZED 17-POINT SCHEME BASED ON THE DIRECTIONAL DERIVATIVE METHOD FOR HIGHLY ACCURATE FINITE-DIFFERENCE SIMULATION OF THE FREQUENCY-DOMAIN 2D SCALAR WAVE EQUATION

WEI LIU[1,2], YANMIN HE[1,2], SHU LI[1,3], HAO WU[1,2], LIFENG YANG[1,2] and ZHENMING PENG[1,2]

[1] School of Information and Communication Engineering, University of Electronic Science and Technology of China, Chengdu 610054, P.R. China.
zmpeng@uestc.edu.cn; davidliuwei@163.com
[2] Information Geoscience Research Center, University of Electronic Science and Technology of China, Chengdu 610054, P.R. China. zmpeng@uestc.edu.cn
[3] School of Information Science and Engineering, Jishou University, Jishou 416000, P.R. China.

(Received March 30, 2018; revised version accepted November 8, 2018)

ABSTRACT

Liu, W., He, Y.M., Li, S, Wu, H., Yang, L.F. and Peng, Z.M., 2019. A generalized 17-point scheme based on the directional derivative method for highly accurate finite-difference simulation of the frequency-domain 2D scalar wave equation. *Journal of Seismic Exploration*, 28: 41-71.

Forward modeling of the frequency-domain wave equation represents an essential foundation for full waveform inversion in the frequency domain, the accuracy and efficiency of which rely heavily on the forward modeling method employed. To reduce the numerical dispersion, anisotropy, and number of grids per the shortest wavelength in forward modeling methods, rotating coordinate systems have been successfully applied to establish finite-difference (FD) schemes for the forward modeling of the frequency-domain wave equation. However, rotated optimal FD schemes are incapable of handling rectangular sampling grids, which are ubiquitous in practice. Fortunately, optimal FD schemes based on the average-derivative method (ADM) overcome this restriction on different directional sampling intervals. However, the ADM itself is merely an algebraic approach and therefore does not inherit the geometrical properties of the rotating coordinate system. Based on the principle of a rotating coordinate system, a novel optimal directional derivative method (DDM)-based 4th-order, 17-point FD scheme is developed in this paper for the forward modeling of the frequency-domain, two-dimension scalar wave equation to approximate the spatial derivatives. The conventional

0963-0651/19/$5.00

4th-order, 9-point scheme and rotated optimal 17-point FD scheme can be derived as special cases of the proposed scheme. Compared with the rotated optimal 17-point FD scheme, the proposed scheme is capable of addressing arbitrary rectangular sampling grids, including equal and unequal directional sampling intervals; moreover, the optimized weighted coefficients can reduce the number of grids per the shortest wavelength from 2.56 to less than 2.4 with maximum phase velocity errors of 1%. Furthermore, the proposed scheme is superior to the ADM-based optimal 17-point FD scheme in suppressing numerical dispersion due to the inherited geometrical properties of the rotating coordinate system. A perfectly matched layer boundary condition is applied to the final FD equation to attenuate boundary reflections. Numerical examples demonstrate the validity and adaptability of our 17-point FD scheme.

KEY WORDS: seismic forward modeling, acoustic wave equation, frequency domain, finite difference, numerical dispersion analysis, directional derivative.

INTRODUCTION

Full waveform inversion (FWI) has recently begun to attract more attention from geophysicists as a result of its ideal mathematical basis, high precision and ability to model multiple parameters. Consequently, FWI has become a research focus in the geophysics community (Tarantola, 1984; Virieux and Operto, 2009; Yang et al., 2014) and can be performed in the time domain (Tarantola, 1984; Gauthier et al., 1986), frequency domain (Pratt, 1990, 1999; Pratt and Worthington, 1990a,b; Pratt et al., 1998; Min et al., 2003), and the Laplace domain (Lee et al., 2008; Pyun et al., 2008; Shin and Cha 2008; Ha and Shin, 2012, 2013; Shin et al., 2013) as well as in a hybrid domain (Shin and Cha, 2009; Shin et al., 2010; Kamei et al., 2015). Since forward modeling is an essential foundation of FWI and constitutes the significant computational cost, the accuracy and efficiency of FWI mainly depend on the forward modeling method employed (Brossier et al., 2009; Virieux and Operto, 2009; Liu et al., 2013).

Regardless of whether it is performed in the time, frequency or Laplace domain, FWI cannot be implemented without forward modeling of the wave equation. Forward modeling of the frequency-domain wave equation was initially proposed by Lysmer and Drake (1972) and was performed using a finite-element method. Based on a comparison between finite-difference (FD) and finite-element forward modeling schemes, Marfurt (1984) indicated that numerical modeling in the frequency domain did not exhibit a stability problem. Compared with the forward modeling in the time domain, forward modeling in the frequency domain possesses numerous advantages, including the ability to implement convenient parallel manipulations of multi-frequency and multi-shot computations based on a direct solver, e.g., lower-upper (LU) factorization, the lack of time accumulated errors, the flexible choice of the frequency band (Operto et al.. 2007), and the smooth implementation of wavefield simulations in viscoelastic media (Pratt, 1990). However, the main disadvantage of frequency-domain forward modeling is that it can be performed only implicitly by solving a large set of linear equations, which requires a substantial amount of computer memory. This disadvantage is particularly apparent in three-dimensional (3D) forward modeling, as even the inclusion of additional computing resources cannot improve the calculation efficiency.

In the context of acoustic wave FWI, Pratt and Worthington (1990a) developed the classical 5-point FD scheme for the two-dimensional (2D) frequency-domain scalar wave equation, which does not impose any limitations on the directional sampling intervals. However, this scheme suffers from serious numerical dispersion errors and requires 13 grids per the shortest wavelength to reduce the phase velocity errors to less than 1%. In general, the numerical dispersion errors of frequency-domain forward modeling methods are more severe than those of time-domain forward modeling methods. That is, frequency-domain forward modeling methods require more grids per the shortest wavelength to achieve the same calculation accuracy as time-domain forward modeling methods, meaning the sampling intervals will consequently be smaller (Jo et al*.,* 1996). Therefore, simply diminishing the sampling interval cannot realistically reduce the numerical dispersion and anisotropy in frequency-domain forward modeling schemes, because this approach will increase the computational time and memory consumption.

To improve the calculation accuracy and reduce the number of grids per the shortest wavelength ($G_{\min}$), rotating coordinate systems have been widely used to construct FD schemes for wave equation forward modeling in the frequency domain (Jo et al., 1996; Shin and Sohn, 1998; Štekl and Pratt 1998; Hustedt et al*.,* 2004; Operto et al., 2009; Cao and Chen, 2012). Based on the 45° rotating coordinate system, Jo et al. (1996) developed an optimal 9-point scheme for the scalar wave equation by using conventional 0° and 45° FD operators to approximate the Laplacian and mass acceleration terms and reduced $G_{\min}$ to approximately 4. Subsequently, Shin and Sohn (1998) developed an optimal 25-point scheme by combining the FD operators of 0°, 26.6°, 45°, and 63.4° rotating coordinate systems and reduced $G_{\min}$ to nearly 2.5. Similarly, Cao and Chen (2012) extended the FD operators of 0° and 45° rotating coordinate systems to the 4th-order and proposed a 4th-order, 17-point FD scheme with a higher calculation accuracy and reduced $G_{\min}$ from 5 to approximately 2.56 relative to the conventional 4th-order, 9-point FD scheme.

Although rotating coordinate system-based optimal algorithms are very effective for the forward modeling of the frequency-domain scalar wave equation, all of the abovementioned rotated optimal FD schemes require equal spatial sampling intervals (i.e., a square sampling grid) along the directions of the **X** and **Z** axes, thereby limiting their practical applications due to different directional sampling intervals of the actual models (i.e., rectangular sample grids). Fortunately, numerous scholars have derived effective solutions targeted at rectangular sampling grids. Chen (2012) proposed a new optimal 9-point scheme based on the average-derivative method (ADM) (Chen, 2008), namely, the ADM-based 9-point scheme. This algorithm includes Jo's rotated optimal 9-point scheme (Jo et al., 1996) as a special case. Subsequently, Zhang et al. (2014) generalized the ADM and proposed an ADM 25-point scheme that includes the rotated 25-point scheme (Shin and Sohn, 1998) as a special case. In terms of a 17-point FD stencil, Tang et al. (2015) proposed an ADM 17-point scheme whose $G_{\min}$ was reduced to approximately 2.4 within which the rotated 17-point scheme

(Cao and Chen, 2012) is similarly regarded as a special case. Though the abovementioned optimal FD ADM schemes improved the calculation accuracy to some extent while generalizing their respective rotated optimal schemes, this was achieved only through algebraic manipulation, and the improved schemes forfeited the geometrical properties of the rotating coordinate systems. Therefore, based on the directional derivative method (DDM) (Saenger et al., 2000) and the staggered-grid technique (Štekl and Pratt, 1998), Chen (2013) proposed a new generalized optimal 9-point FD scheme that not only retains the geometrical properties of the rotating coordinate system but also addresses arbitrary rectangular sampling grids with more flexibility. In addition to the commonly used 9-, 25-, and 17-point FD schemes, Liu et al. (2013) proposed a 15-point FD scheme aimed at effectively suppressing dispersions with a smaller impedance-matrix bandwidth (i.e., less memory consumption) and reduced $G_{\min}$ to approximately 2.97. Although only a square sampling grid was discussed, this method can also be applied to rectangular sampling grids. Lately, Fan et al. (2017) developed a more generalized optimal method for the FD simulation of the 2D frequency-domain scalar wave equation, based upon which the dispersion equation and optimal expansion coefficients can be obtained for a given FD stencil and many commonly used frequency-domain FD schemes (e.g., FD stencils with different numbers of points, different directional sampling intervals, and rotated sampling grids) can be derived as special cases. Although the optimal 25-point scheme based on this algorithm has a much higher accuracy than the ADM 25-point scheme (Zhang et al., 2014), and though its $G_{\min}$ is reduced from 2.78 to 2.13, the corresponding improvements for the corresponding ADM 9-, 17-, and 15-point FD schemes are trivial.

In general, improving the FD scheme is an effective way to increase the accuracy and efficiency of wave equation forward modeling in the frequency domain. Rotating coordinate systems have been successfully applied to wave equation forward modeling in the frequency domain; moreover, the improved ADM-based FD schemes can overcome defects in rotated optimal FD schemes, and they can be employed with different directional sampling intervals. Despite these qualities, however, the abovementioned ADM schemes (except for the ADM 17- and 25-point schemes) cannot produce high-precision images from seismic exploration due to their 2nd-order accuracy and lack of geometrical properties related to the rotating coordinate system. In this paper, a novel DDM-based 17-point scheme with a 4th-order accuracy is developed for the frequency-domain scalar wave equation. Theoretical analyses show that this new scheme retains the geometrical properties of the rotating coordinate system and that it can be flexibly applied to arbitrary rectangular sampling grids in practice. Numerical dispersion analyses reveal that the DDM 17-point scheme reduces $G_{\min}$ to less than 2.4 and can decrease the required computer memory and maintain the same accuracy by increasing the sampling interval. Numerical simulation examples further prove that our scheme can effectively suppress numerical dispersion and anisotropy and improve the calculation accuracy. Finally, we provide a valid and adaptable forward modeling method for high-precision FWI in the frequency domain.

THEORY

Conventional 17-point scheme and its limitations

In a Cartesian coordinate system, the frequency-domain 2D scalar wave equation for a homogeneous medium is given by

$$\nabla^2 P\left(\mathbf{x},\omega\right)+\frac{\omega^2}{v^2}P\left(\mathbf{x},\omega\right)=-F\left(\omega\right)\delta\left(\mathbf{x}-\mathbf{s}\right) \quad , \tag{1}$$

where $P\left(\mathbf{x},\omega\right)$ is the frequency-domain wavefield pressure, $F\left(\omega\right)$ is the Fourier transform of the source function, ω is the angular frequency, $\delta\left(\mathbf{x}\right)$ is the Dirac delta function, $v\left(\mathbf{x}\right)$ is the propagation velocity of the seismic wave, $\mathbf{x}=\left(x,z\right)$ and $\mathbf{s}=\left(x_s,z_s\right)$ are the spatial coordinates and the coordinates of the source location, respectively, and $\nabla^2=\frac{\partial^2}{\partial x^2}+\frac{\partial^2}{\partial z^2}$ is the 2nd-order differential operator. The first term on the left-hand side of eq. (1) is known as the Laplacian term, and the second term is known as the mass acceleration term.

Due to their low precision and heavy numerical dispersion, frequency-domain, 2nd-order FD schemes need smaller grid intervals to improve the accuracy of forward modeling. Meanwhile, frequency-domain, 4th-order FD schemes, such as the conventional 4th-order 9-point and 17-point schemes whose FD stencils are shown in Fig. 1, exhibit higher precisions.

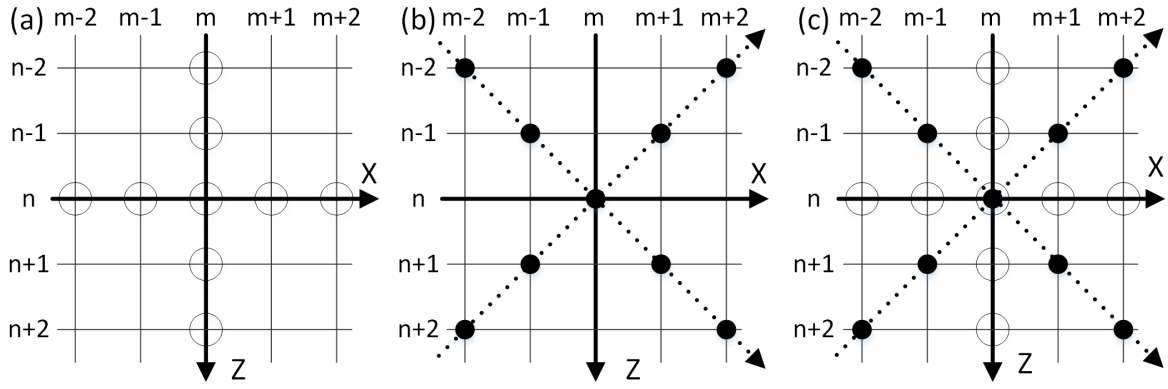

Fig. 1. Finite-difference (FD) grid stencil for the Laplacian operator of (a) the conventional 4th-order, 9-point scheme, (b) the 45° rotated stencil, and (c) the conventional 4th-order, 17-point scheme.

Applying the 4th-order central FD operator to approximate the 2nd-order spatial derivative (i.e., the Laplacian term) in eq. (1), the conventional 4th-order, 9-point FD scheme can be written as

$$\begin{aligned}&\frac{-1/12\left(P_{m-2,n}+P_{m+2,n}\right)+4/3\left(P_{m-1,n}+P_{m+1,n}\right)-5/2\,P_{m,n}}{\Delta x^2}+\\&\frac{-1/12\left(P_{m,n-2}+P_{m,n+2}\right)+4/3\left(P_{m,n-1}+P_{m,n+1}\right)-5/2\,P_{m,n}}{\Delta z^2}+\frac{\omega_j^2}{v_{m,n}^2}P_{m,n}=0,\end{aligned}\tag{2}$$

where $P_{m,n}=P\left(m\Delta x,n\Delta z\right)$ is the discretized wavefield, $v_{m,n}=v\left(m\Delta x,n\Delta z\right)$ is the discretized velocity, Δx and Δz are the spatial sampling intervals along the **X** and **Z** axis directions, respectively, m and n are the sequence numbers of the **X** and **Z** axis coordinates, respectively, and j is the sequence number of the frequency.

Based on eq. (2), Cao and Chen (2012) generalized the Laplacian term as a linear combination of the 4th-order FD approximations for the Laplacian operators of the 45° rotating coordinate system and original 0° rectangular coordinate system and formulated the wavefield pressure of mass acceleration term as a linear combination of the wavefield pressures at the points corresponding to the Laplacian term. Then, the 4th-order, 17-point FD scheme can be given by

$$\begin{aligned}&a\left[\frac{-1/12\left(P_{m-2,n}+P_{m+2,n}\right)+4/3\left(P_{m-1,n}+P_{m+1,n}\right)-5/2\,P_{m,n}}{\Delta x^2}\right.\\&\left.+\frac{-1/12\left(P_{m,n-2}+P_{m,n+2}\right)+4/3\left(P_{m,n-1}+P_{m,n+1}\right)-5/2\,P_{m,n}}{\Delta z^2}\right]+\\&(1-a)\left[\frac{-1/12\left(P_{m-2,n-2}+P_{m+2,n+2}\right)+4/3\left(P_{m-1,n-1}+P_{m+1,n+1}\right)-5/2\,P_{m,n}}{\Delta x^2+\Delta z^2}\right.\\&\left.+\frac{-1/12\left(P_{m+2,n-2}+P_{m-2,n+2}\right)+4/3\left(P_{m+1,n-1}+P_{m-1,n+1}\right)-5/2\,P_{m,n}}{\Delta x^2+\Delta z^2}\right]+\\&\frac{\omega_j^2}{v_{m,n}^2}\left[bP_{m,n}+c\left(P_{m-1,n}+P_{m+1,n}+P_{m,n-1}+P_{m,n+1}\right)+d\left(P_{m-1,n-1}+P_{m+1,n+1}+P_{m-1,n+1}+P_{m+1,n-1}\right)\right.\\&\left.+e\left(P_{m-2,n}+P_{m+2,n}+P_{m,n-2}+P_{m,n+2}\right)+f\left(P_{m-2,n-2}+P_{m+2,n+2}+P_{m-2,n+2}+P_{m+2,n-2}\right)\right]=0,\end{aligned}\tag{3}$$

where the constants a, b, c, d, e, and f are the weighted coefficients that can be obtained via an optimization approach, and $b+4(c+d+e+f)=1$. In eq. (3) the first and second terms on the left-hand side are the FD approximations for the Laplacian operators of the 0° rectangular coordinate system and 45° rotating coordinate system, respectively.

In the case where $\Delta x = \Delta z$, the coefficients used in the 4th-order, 17-point scheme are optimized through numerical dispersion analysis (Cao and Chen 2012) as a = 1.0673, b = 0.8875, c = 0.0251, d = 0.0237, e = –0.0204, and f = –0.000275. This scheme can reduce $G_{\min}$ to less than 2.56 and decrease the numerical dispersion and memory requirement, while the conventional 4th-order, 9-point scheme needs at least 5 grids per the shortest wavelength. Unfortunately, the 4th-order, 17-point scheme fails because the directional sampling intervals are unequal in most cases. When $\Delta x \neq \Delta z$, the second term on the left-hand side of eq. (3) is not an approximation for the Laplacian term.

If the second term on the left-hand side of eq. (3) is expanded using Taylor's formula for the binary function, we can obtain

$$\begin{aligned}&\frac{-\frac{1}{12}\left(P_{m-2,n-2}+P_{m+2,n+2}\right)+\frac{4}{3}\left(P_{m-1,n-1}+P_{m+1,n+1}\right)-\frac{5}{2}P_{m,n}}{\Delta x^2+\Delta z^2}+\\&\frac{-\frac{1}{12}\left(P_{m+2,n-2}+P_{m-2,n+2}\right)+\frac{4}{3}\left(P_{m+1,n-1}+P_{m-1,n+1}\right)-\frac{5}{2}P_{m,n}}{\Delta x^2+\Delta z^2}=\\&\frac{2\Delta x^2}{\Delta x^2+\Delta z^2}\frac{\partial^2 P}{\partial x^2}\Big|_{m,n}+\frac{2\Delta z^2}{\Delta x^2+\Delta z^2}\frac{\partial^2 P}{\partial z^2}\Big|_{m,n}+o\left(\Delta x^2,\Delta z^2\right).\end{aligned} \tag{4}$$

From eq. (4), the FD operator of a 45° rotating coordinate system is an approximation for the Laplacian term only when $\Delta x = \Delta z$. The detailed derivation is referred to in the Appendix.

A directional derivative method-based 17-point scheme

To improve the calculation accuracy and reduce the memory requirements, we developed a novel optimal 4th-order, 17-point scheme based on the DDM (Saenger et al., 2000) with the ambition of overcoming the obstacles of the rotated optimal 4th-order, 17-point scheme (Cao and Chen, 2012). When $\Delta x \neq \Delta z$, the principle of a rotating coordinate system can be generalized to a DDM, which has been successfully applied to the development of the rotated optimal 2nd-order, 9-point scheme (Chen, 2013).

When $\Delta x \neq \Delta z$, the two axis directions $\mathbf{L}_1$ and $\mathbf{L}_2$ of the rotating coordinate system are not orthogonal to each other. That is, the included angle between the two axis directions is less than 90°. Thus, we call this

rotating coordinate system the diagonal coordinate system in this paper. The relationship between the diagonal coordinate system and the original rectangular coordinate system is shown in Fig. 2. We can compute the 1st-order directional derivatives $\frac{\partial P}{\partial l_1}$ and $\frac{\partial P}{\partial l_2}$ as follows:

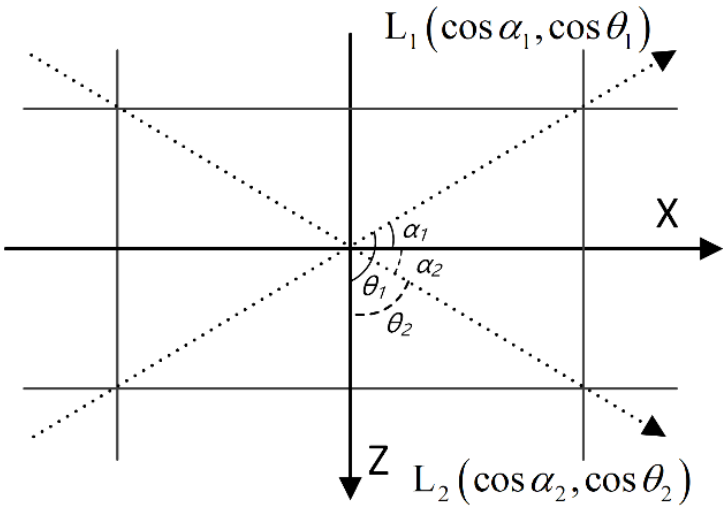

Fig. 2. Schematic of the relationship between the diagonal coordinate system and the original rectangular coordinate system.

$$\begin{aligned}\frac{\partial P}{\partial l_1} &= \cos\alpha_1 \frac{\partial P}{\partial x} + \cos\theta_1 \frac{\partial P}{\partial z},\\ \frac{\partial P}{\partial l_2} &= \cos\alpha_2 \frac{\partial P}{\partial x} + \cos\theta_2 \frac{\partial P}{\partial z},\end{aligned} \tag{5}$$

where

$$\cos\alpha_1 = \cos\alpha_2 = \frac{\Delta x}{\Delta l},\quad \cos\theta_1 = -\frac{\Delta z}{\Delta l},\quad \cos\theta_2 = \frac{\Delta z}{\Delta l}, \tag{6}$$

$\Delta l = \sqrt{\Delta x^2 + \Delta z^2}$, l_1 and l_2 are the variables along the two axis directions in the diagonal coordinate system, α_1 and θ_1 are the included angles between the direction of $\mathbf{L}_1$ and the positive directions of the **X** and **Z** axes, respectively, and α_2 and θ_2 are similarly the included angles between the direction of $\mathbf{L}_2$ and the positive directions of the **X** and **Z** axes. With eqs. (5) and (6), we can obtain the 2nd-order directional derivatives as follows:

$$\begin{aligned}
\frac{\partial^2 P}{\partial l_1^2} &= \frac{\Delta x^2}{\Delta l^2}\frac{\partial^2 P}{\partial x^2} + \frac{\Delta z^2}{\Delta l^2}\frac{\partial^2 P}{\partial z^2} - 2\frac{\Delta x \Delta z}{\Delta l^2}\frac{\partial^2 P}{\partial x \partial z}, \\
\frac{\partial^2 P}{\partial l_2^2} &= \frac{\Delta x^2}{\Delta l^2}\frac{\partial^2 P}{\partial x^2} + \frac{\Delta z^2}{\Delta l^2}\frac{\partial^2 P}{\partial z^2} + 2\frac{\Delta x \Delta z}{\Delta l^2}\frac{\partial^2 P}{\partial x \partial z}, \\
\frac{\partial^2 P}{\partial l_1 \partial l_2} &= \frac{\Delta x^2}{\Delta l^2}\frac{\partial^2 P}{\partial x^2} - \frac{\Delta z^2}{\Delta l^2}\frac{\partial^2 P}{\partial z^2}.
\end{aligned} \tag{7}$$

With eq. (7), we can further obtain the expression of the Laplacian term including directional derivatives:

$$\frac{\partial^2 P}{\partial x^2} + \frac{\partial^2 P}{\partial z^2} = \frac{\Delta l^2\left(\Delta z^2 + \Delta x^2\right)}{4\Delta x^2 \Delta z^2}\left(\frac{\partial^2 P}{\partial l_1^2} + \frac{\partial^2 P}{\partial l_2^2}\right) + \frac{\Delta l^2\left(\Delta z^2 - \Delta x^2\right)}{2\Delta x^2 \Delta z^2}\frac{\partial^2 P}{\partial l_1 \partial l_2}. \tag{8}$$

Applying the 4th-order central FD operator to eq. (8), an approximation to the Laplacian term can be obtained:

$$\begin{aligned}
\frac{\partial^2 P}{\partial x^2}\Big|m,n + \frac{\partial^2 P}{\partial z^2}\Big|m,n = \frac{\Delta z^2 + \Delta x^2}{4\Delta x^2 \Delta z^2}\Big[&\frac{4}{3}\left(P_{m+1,n-1} + P_{m-1,n+1} + P_{m-1,n-1} + P_{m+1,n+1}\right) \\
&- \frac{1}{12}\left(P_{m+2,n-2} + P_{m-2,n+2} + P_{m-2,n-2} + P_{m+2,n+2}\right) - 5P_{m,n}\Big] \\
&+ \frac{\left(\Delta z^2 - \Delta x^2\right)}{2\Delta x^2 \Delta z^2}\Big[\Big(\frac{4}{3}\left(P_{m+1,n} + P_{m-1,n} - P_{m,n+1} - P_{m,n-1}\right) \\
&- \frac{1}{12}\left(P_{m+2,n} + P_{m-2,n} - P_{m,n+2} - P_{m,n-2}\right)\Big].
\end{aligned} \tag{9}$$

Combining eq. (9) with eq. (2) and representing the wavefield pressure of mass acceleration term as a linear combination of the wavefield pressures at the points corresponding to the Laplacian term, the optimal 4th-order, 17-point DDM-based scheme can be obtained:

$$a\left[\begin{array}{l}\dfrac{4/3\left(P_{m+1,n}+P_{m-1,n}\right)-1/12\left(P_{m+2,n}+P_{m-2,n}\right)-5/2P_{m,n}}{\Delta x^2}+\\ \dfrac{4/3\left(P_{m,n+1}+P_{m,n-1}\right)-1/12\left(P_{m,n+2}+P_{m,n-2}\right)-5/2P_{m,n}}{\Delta z^2}\end{array}\right]$$

$$(1-a)\left[\frac{1}{\bar{\Delta}^2}\left(\begin{array}{l}4/3\left(P_{m+1,n-1}+P_{m-1,n+1}+P_{m-1,n-1}+P_{m+1,n+1}\right)-\\ 1/12\left(P_{m+2,n-2}+P_{m-2,n+2}+P_{m-2,n-2}+P_{m+2,n+2}\right)-5P_{m,n}\end{array}\right)+\bar{P}_{m,n}\right]+$$

$$\frac{\omega_j^2}{v_{m,n}^2}\left[b_1P_{m,n}+b_2\left(P_{m-1,n}+P_{m+1,n}\right)+b_3\left(P_{m,n-1}+P_{m,n+1}\right)+b_4\left(P_{m-2,n}+P_{m+2,n}\right)+b_5\left(P_{m,n-2}+P_{m,n+2}\right)\right.$$

$$\left.+b_6\left(P_{m+1,n-1}+P_{m-1,n+1}+P_{m-1,n-1}+P_{m+1,n+1}\right)+b_7\left(P_{m+2,n-2}+P_{m-2,n+2}+P_{m-2,n-2}+P_{m+2,n+2}\right)\right]=0, \tag{10}$$

where

$$\bar{\Delta}=2/\sqrt{1/\Delta x^2+1/\Delta z^2},$$

$$\bar{P}_{m,n}=\frac{\Delta z^2-\Delta x^2}{2\Delta x^2\Delta z^2}\left(\begin{array}{l}4/3\left(P_{m+1,n}+P_{m-1,n}-P_{m,n+1}-P_{m,n-1}\right)-\\ 1/12\left(P_{m+2,n}+P_{m-2,n}-P_{m,n+2}-P_{m,n-2}\right)\end{array}\right), \tag{11}$$

where the constants a, $b_i\left(i=1,\mathrm{L}\ ,7\right)$ are the weighted coefficients for optimization, and $b_1+2\sum_{i=2}^{5}b_i+4\sum_{i=6}^{7}b_i=1$.

Compared with the conventional rotated optimal 17-point scheme, the proposed scheme is a more generalized optimal 4th-order, 17-point scheme with a wider application range that includes square sampling grids and arbitrary rectangular sampling grids. When $\Delta x=\Delta z$, $b_2=b_3$, $b_4=b_5$, eq. (10) degrades to eq. (3); that is, the new 17-point scheme includes the rotating coordinate system-based 17-point scheme as a special case. In addition, when $a=b_1=1$ and $b_i=0\left(i=2,\mathrm{L}\ ,7\right)$, the classical 4th-order, 9-point scheme is included in the proposed 17-point scheme as another special case.

Coefficient optimization and dispersion analysis

To obtain synthetic seismograms with a high precision, numerical dispersion and anisotropy issues in forward modeling methods must be reduced optimally (Alford et al., 1974). To this end, numerical dispersion analysis can be used to evaluate the precision of a forward modeling method,

and the optimal coefficients required to minimize the normalized phase velocities or dispersion errors can be determined via optimization.

To perform numerical dispersion analysis for the proposed scheme, we substituted a plane wave $P(x,z,\omega)=P_0e^{-i(k_xx+k_zz)}$ into eq. (10). Assuming the velocity v of the medium is a constant, the discrete dispersion relation can be derived as

$$\frac{\omega^2}{v^2}=\frac{\frac{a}{6}\left[15\left(\Delta x^2+\Delta z^2\right)-16\left(A\Delta z^2+C\Delta x^2\right)+\left(B\Delta z^2+D\Delta x^2\right)\right]+\frac{1-a}{12}\left[\left(\Delta x^2+\Delta z^2\right)\left(15+BD-16AC\right)+\left(\Delta z^2-\Delta x^2\right)\left(\left(B-D\right)-16\left(A-C\right)\right)\right]}{\Delta x^2\Delta z^2\left(b_1+2b_2A+2b_3C+2b_4B+2b_5D+4b_6AC+4b_7BD\right)}, \tag{12}$$

where

$$A=\cos\left(k_x\Delta x\right),B=\cos\left(2k_x\Delta x\right),C=\cos\left(k_z\Delta z\right),D=\cos\left(2k_z\Delta z\right). \tag{13}$$

From the definition of the phase velocity $v_{ph}=\omega/k$, the normalized phase velocity can be obtained as

$$\frac{v_{ph}}{v}=\frac{\left\{\frac{a}{6}\left[15\left(\Delta x^2+\Delta z^2\right)-16\left(A\Delta z^2+C\Delta x^2\right)+\left(B\Delta z^2+D\Delta x^2\right)\right]+\frac{1-a}{12}\left[\left(\Delta x^2+\Delta z^2\right)\left(15+BD-16AC\right)+\left(\Delta z^2-\Delta x^2\right)\left(\left(B-D\right)-16\left(A-C\right)\right)\right]\right\}^{1/2}}{k\Delta x\Delta z\left(b_1+2b_2A+2b_3C+2b_4B+2b_5D+4b_6AC+4b_7BD\right)^{1/2}}, \tag{14}$$

where $k=2\pi/\lambda=2\pi/G\Delta$ is the plane wave wavenumber, $k_x=k\sin\theta$ and $k_x=k\cos\theta$ are the wavenumbers of the plane wave along the **X** and **Z** axis directions, respectively, θ is the propagation angle from the positive direction of the **Z** axis, $G=\lambda/\Delta$ is defined as the number of grids per wavelength λ, and $\Delta=\max\left(\Delta x,\Delta z\right)$ is the largest sampling interval, that is, the value of G is determined by the grid interval of the rectangular sampling grid. Thus, the numerical dispersion analysis and coefficient optimization should be separated into two conditions: $\Delta x\geq\Delta z$ and $\Delta x<\Delta z$.

We first consider the condition $\Delta x\geq\Delta z$. Substituting the sampling interval ratio $r=\Delta x/\Delta z$ and the wavenumber $k=2\pi/G\Delta x$ into eq. (14), the normalized phase velocity can be expressed as

$$\frac{v_{ph}}{v}\Big|_{\Delta x\geq\Delta z}=\frac{\left\{\frac{a}{6}\left[15\left(1+r^2\right)-16\left(A+Cr^2\right)+\left(B+Dr^2\right)\right]+\frac{1-a}{12}\left[\left(1+r^2\right)\left(15+BD-16AC\right)+\left(1-r^2\right)\left(\left(B-D\right)-16\left(A-C\right)\right)\right]\right\}^{1/2}}{\frac{2\pi}{G}\left(b_1+2b_2A+2b_3C+2b_4B+2b_5D+4b_6AC+4b_7BD\right)^{1/2}}, \tag{15}$$

where

$$\begin{aligned} A &= \cos\left(k_x \Delta x\right) = \cos\left(\tfrac{2\pi}{G}\sin\theta\right), B = \cos\left(2k_x \Delta x\right) = \cos\left(\tfrac{4\pi}{G}\sin\theta\right), \\ C &= \cos\left(k_z \Delta z\right) = \cos\left(\tfrac{2\pi}{G}\cos\theta\right), D = \cos\left(2k_z \Delta z\right) = \cos\left(\tfrac{4\pi}{G}\cos\theta\right). \end{aligned} \tag{16}$$

There is no numerical dispersion when the numerical phase velocity is equal to that of the medium, namely, $\frac{v_{ph}}{v} = 1$ (Jo et al., 1996). Under 2D conditions, numerical dispersion is related to the propagation angle of the seismic wave, the sampling grid interval and the coefficients in eq. (10). Therefore, the weighted coefficients a, b_i (i = 1,…,7) can be obtained by minimizing the L2-norm of the normalized phase velocity errors (i.e., a dispersion analysis objective function), which is defined as follows:

$$E\left(r; a, b_i\right) = \iint \left(1 - \frac{v_{ph}}{v}\left(r; a, b_i; \theta, k^*\right)\right)^2 d\theta dk^*, \; i = 1, \mathrm{K}\,, 7, \tag{17}$$

where $k^* = 1/G = \Delta/\lambda$. Substituting eq. (15) into eq. (17), the objective functions for different sampling interval ratios $r = \Delta x/\Delta z$ can be obtained.

To obtain the optimal values of the coefficients a and $b_i\left(i = 1, \mathrm{L}\,, 7\right)$, a constrained global optimization algorithm (Global Search) in MATLAB was used to solve the objective functions. The range of $k^* = 1/G$ can usually be determined practically via multiplicate trials; here, the range is $\left(0, 0.435\right]$ with an interval of 0.001. Moreover, the range of the propagation angle θ is $\left[0°, 90°\right]$ with an interval of 1°.

The optimized coefficients for different sampling interval ratios $r = \Delta x/\Delta z$ are listed in Table 1 when $\Delta x \geq \Delta z$. When $r > 1.0$ in Table 1, the absolute values of the optimization coefficients a, b_1 and b_7 increase with an increasing ratio, whereas the absolute values of the optimization coefficients b_2 and b_4 show a downward trend. Meanwhile, the change patterns for the absolute values of the optimization coefficients b_3, b_5 and b_6 are the same with an initial decreasing trend followed by an increasing trend, and they reach their minimum values at approximately 2.0. For $\Delta x < \Delta z$ and $k = 2\pi/G\Delta z$, the optimized coefficients for the different sampling interval ratios $r = \Delta z/\Delta x$ can be obtained through the same procedures as in the case of $\Delta x \geq \Delta z$ (Table 1). Through a comparison of the optimization coefficients in Table 1 and Table 2, the values of the coefficients a, b_1, b_6 and b_7 are the same while the values of the coefficients b_2 and b_4 are exchanged with those of the coefficients b_3 and b_5, respectively, as is determined by the symmetry of the DDM 17-point scheme. Although only the optimization coefficients related to a part of the sampling interval ratios are provided in this paper, the optimization coefficients for the remaining sampling interval ratios can be easily obtained using the same approach.

Table 1. The optimized coefficients for different sampling interval ratios $r = \Delta x/\Delta z$ when $\Delta x \geq \Delta z$.

$r=\Delta x/\Delta z$	a	b1	b2	b3	b4	b5	b6	b7
1.0	1.4294927	0.9943091	-0.0234205	-0.0234199	-0.0279369	-0.0279374	0.0505651	0.0022150
1.5	0.6992809	0.7854866	**0.0837901**	**0.0600050**	**-0.0183311**	**-0.0068620**	-0.0024708	-0.0032019
2.0	0.7163125	0.8302360	**0.0781348**	**0.0289988**	**-0.0174147**	**0.0020851**	0.0000659	-0.0035269
2.5	0.7227821	0.9054697	**0.0717649**	**-0.0230907**	**-0.0157992**	**0.0166854**	0.0031150	-0.0042627
3.0	0.7254346	1.0354868	**0.0644372**	**-0.1124488**	**-0.0136899**	**0.0410985**	0.0067086	-0.0052788
3.5	0.7261739	1.2444166	**0.0567076**	**-0.2552140**	**-0.0111873**	**0.0794327**	0.0105308	-0.0065044
4.0	0.7266541	1.5631476	**0.0476554**	**-0.4717152**	**-0.0082623**	**0.1365899**	0.0150302	-0.0079510

Table 2. The optimized coefficients for different sampling interval ratios $r = \Delta z/\Delta x$ when $\Delta x < \Delta z$.

$r=\Delta z/\Delta x$	a	b1	b2	b3	b4	b5	b6	b7
1.5	0.6992809	0.7854866	**0.0600050**	**0.0837901**	**-0.0068620**	**-0.0183311**	-0.0024708	-0.0032019
2.0	0.7163125	0.8302360	**0.0289988**	**0.0781348**	**0.0020851**	**-0.0174147**	0.0000659	-0.0035269
2.5	0.7227821	0.9054697	**-0.0230907**	**0.0717649**	**0.0166854**	**-0.0157992**	0.0031150	-0.0042627
3.0	0.7254346	1.0354868	**-0.1124488**	**0.0644372**	**0.0410985**	**-0.0136899**	0.0067086	-0.0052788
3.5	0.7261739	1.2444166	**-0.2552140**	**0.0567076**	**0.0794327**	**-0.0111873**	0.0105308	-0.0065044
4.0	0.7266541	1.5631476	**-0.4717152**	**0.0476554**	**0.1365899**	**-0.0082623**	0.0150302	-0.0079510

The following content concerns numerical dispersion analysis. When $\Delta x \geq \Delta z$, Figs. 3–6 show the normalized phase velocity curves (dispersion curves) of the conventional 4th-order, 9-point scheme, rotated optimal 17-point scheme, and the ADM 17-point scheme in addition to our DDM 17-point scheme for different sampling interval ratios $r = \Delta x/\Delta z$. As shown in Fig. 3, when r =1.0 ($\Delta x = \Delta z$), numerical dispersion is most likely to occur with a phase velocity error of ±1% in the conventional 4th-order, 9-point scheme, which has no optimization and requires 5 grids per the shortest wavelength compared with the other three optimized 17-point schemes. Furthermore, the differences among the dispersion curves for the different propagation directions are very apparent and lead to evident anisotropy. Nevertheless, the ADM 17-point scheme and the DDM 17-point scheme exhibit slighter numerical dispersion and anisotropy and only require 2.4 grids per the shortest wavelength for maximum phase velocity errors of 1%,

while the rotated 4th-order, 17-point scheme needs at least 2.56 grids (Cao and Chen, 2012). It is noteworthy that a seismic wave propagating in the 45° direction will exhibit the smallest numerical dispersion because its dispersion curve fluctuates slightly around 1.0 for most values of $1/G$. However, seismic waves propagating in the vertical (0°) and horizontal (90°) directions are the most likely to yield obvious numerical dispersion due to the more apparent fluctuations in their dispersion curves. Moreover, the dispersion curves of seismic waves propagating in the 0°, 15° and 30° directions coincide with those propagating in the 90°, 75° and 60° directions, respectively. Therefore, the normalized phase velocity errors are symmetric about that of a wave propagating in the 45° direction in the angle range of 0°–90°; this feature also exists in the other ranges of propagation angles as a result of symmetry in the 17-point schemes when $\Delta x = \Delta z$.

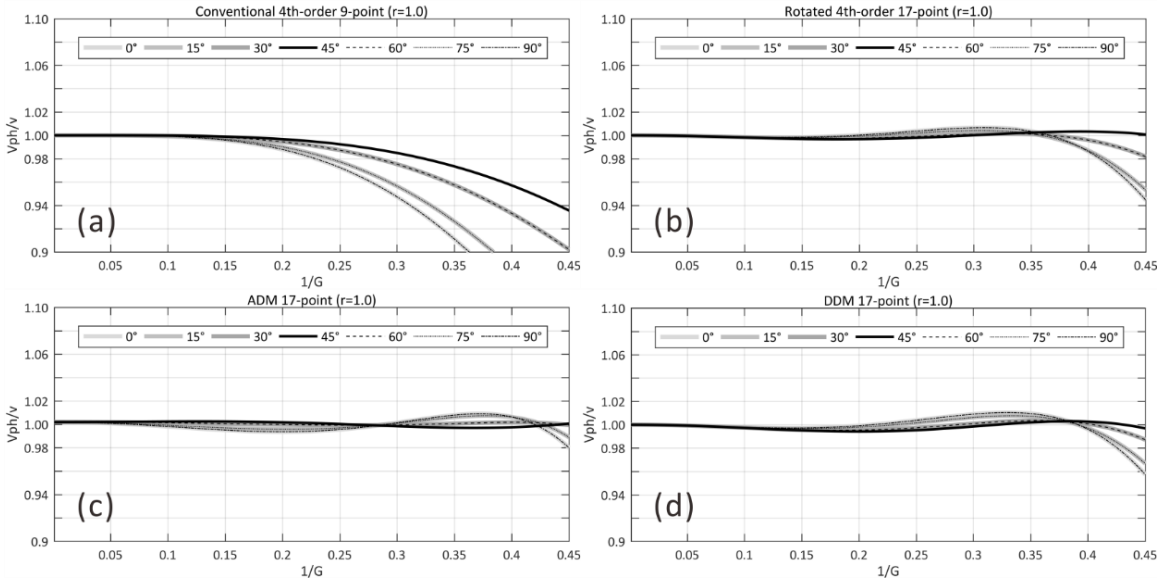

Fig. 3. Normalized phase velocity curves of the conventional 4th-order, 9-point (a) and 17-point (b) schemes and the ADM-based 17-point (c) and DDM-based 17-point schemes (d) when $\Delta x = \Delta z$.

When $\Delta x > \Delta z$, the dispersion curves of the conventional 4th-order, 9-point scheme, the ADM 17-point scheme and the proposed DDM 17-point scheme for different sampling interval ratios $r = \Delta x/\Delta z$ are as shown in Figs. 4-5.

When $\Delta x > \Delta z$, the normalized phase velocity errors are no longer symmetrical, and the propagation angle of the seismic wave with the smallest dispersion does not approach 45° but instead gradually approaches 0°. In terms of the classical 4th-order, 9-point scheme, the seismic waves with larger propagation angles cause numerical dispersion more easily within the propagation angle range of 0°–90°. The dispersion curves of the ADM 17-point and DDM 17-point schemes do not change with variations in the values of the ratio r because of the optimization process, whereas the seismic waves with larger propagation angles are also more likely to exhibit numerical dispersion as a result of the extended horizontal sampling interval.

Compared with the ADM 17-point scheme, the proposed DDM 17-point scheme demonstrates superior dispersion suppression capabilities. Specifically, all of the dispersion curves of the DDM 17-point scheme for seismic waves propagating along different angles exhibit smaller fluctuations, especially those with much larger propagation angles. Furthermore, when $1/G_{\min} \le 0.25$, the normalized phase velocity errors of the DDM 17-point scheme are distributed more closely to 1.0, which means there is little dispersion in our DDM 17-point scheme. In contrast, the ADM 17-point scheme is still likely to yield apparent dispersion, especially at approximately $1/G \in [0.1, 0.25]$. For $\Delta x < \Delta z$, analogous conclusions with respect to numerical dispersion and the number of grids per the shortest wavelength can be drawn due to the symmetry of the DDM 17-point scheme; consequently, those conclusions will not be presented here in this paper.

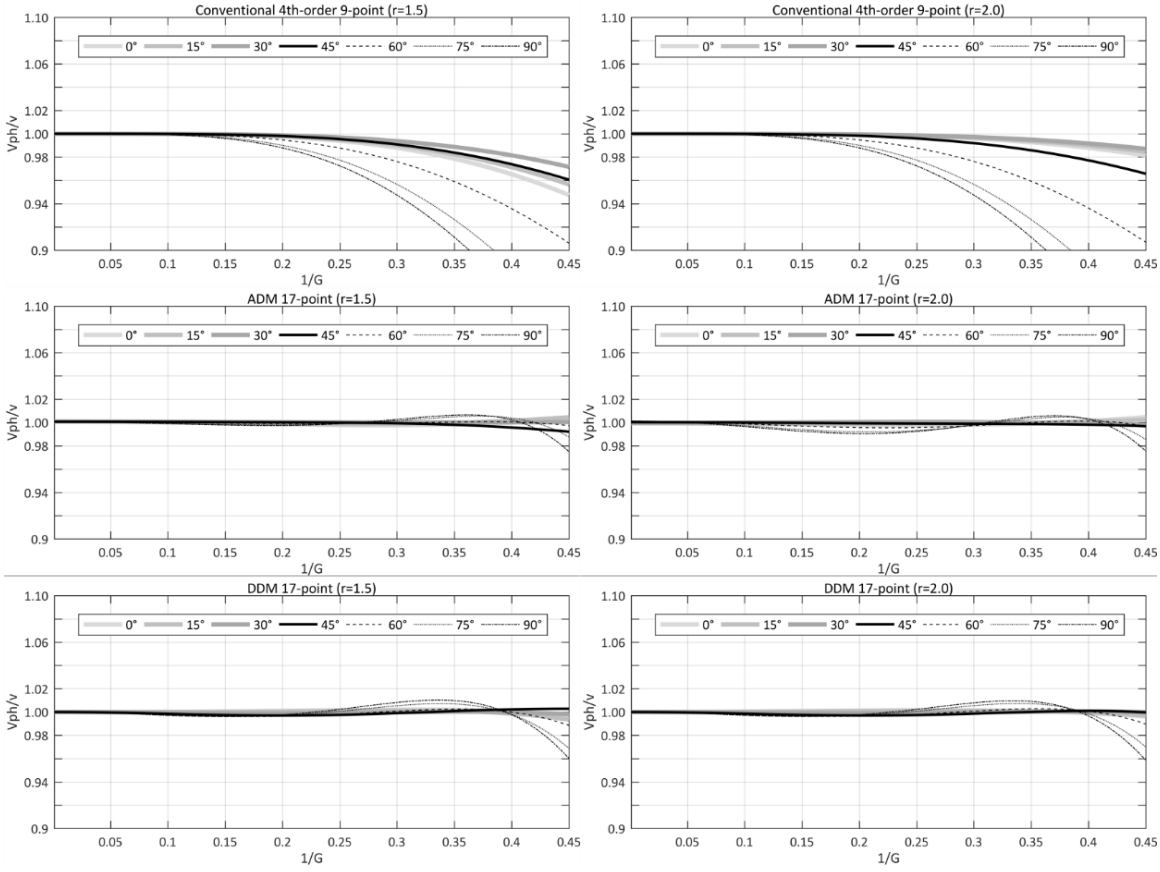

Fig. 4. Normalized phase velocity curves of the conventional 4th-order, 9-point scheme, the ADM-based 17-point scheme and the DDM-based 17-point scheme when $r = 1.5$ (left column) and $r = 2.0$ (right column).

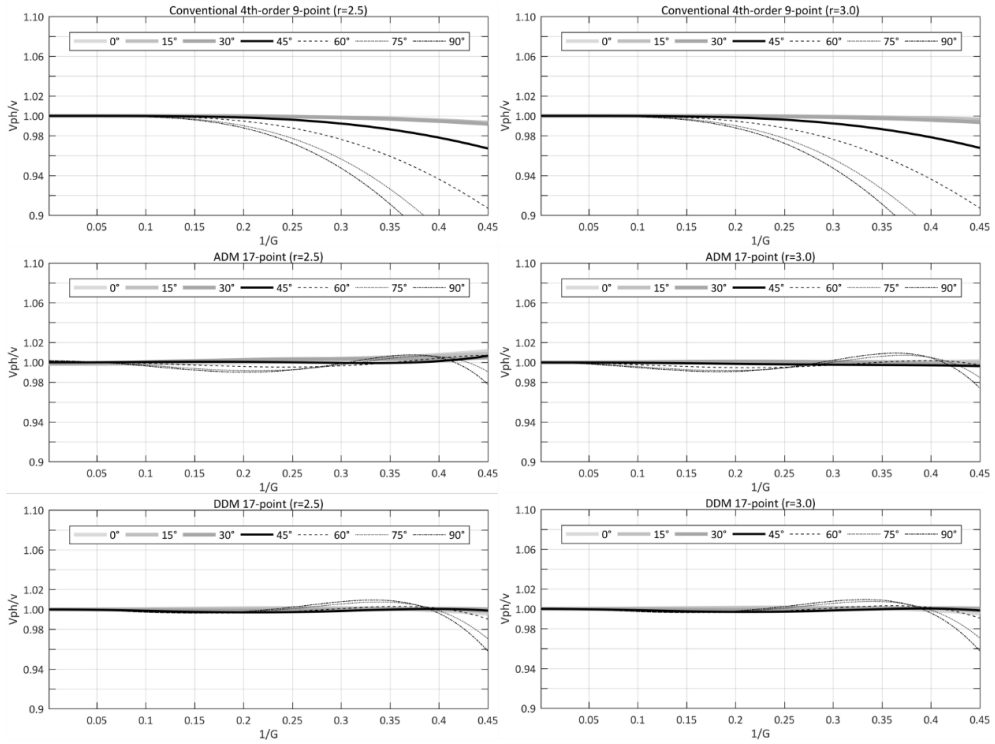

Fig. 5. Normalized phase velocity curves of the conventional 4th-order, 9-point scheme, the ADM-based 17-point and the DDM-based 17-point scheme when $r = 2.5$ (left column) and $r = 3.0$ (right column).

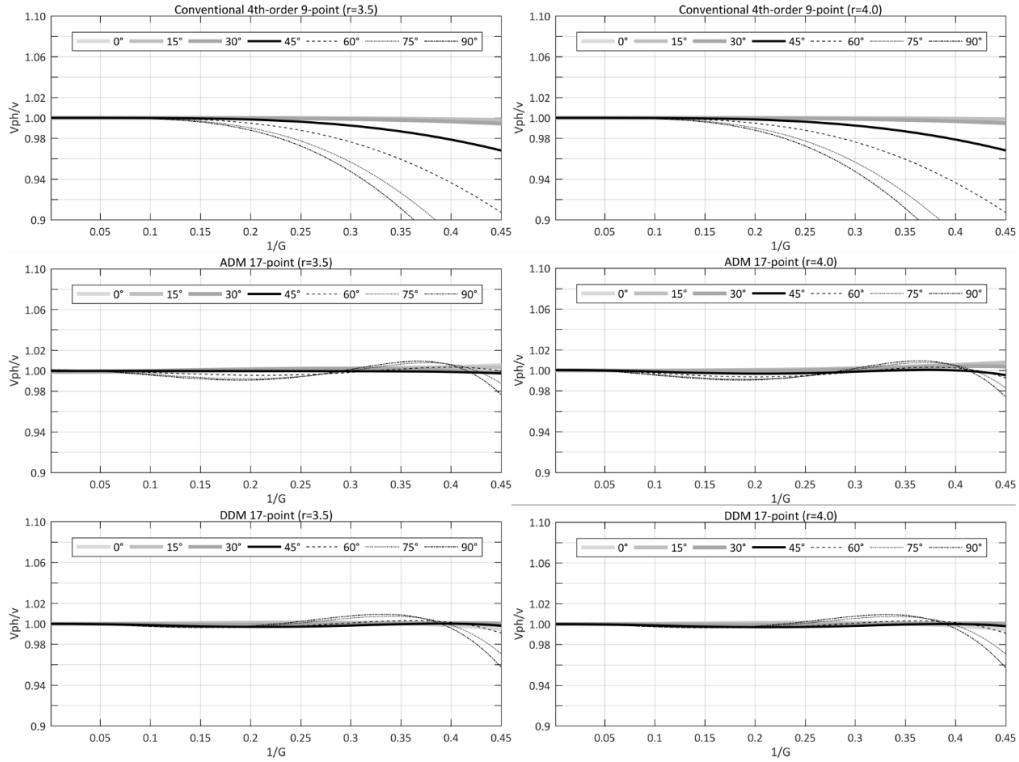

Fig. 6. Normalized phase velocity curves of the conventional 4th-order, 9-point scheme, the ADM-based 17-point and the DDM-based 17-point scheme when $r = 3.5$ (left column) and $r = 4.0$ (right column).

Absorptive boundary conditions

The suppression effects of absorptive boundary conditions for boundary reflections can influence the forward modeling accuracy. The perfectly matched layer (PML) absorbing boundary condition was pioneered by Bérenger (1994), and it has been widely used for FD simulations of the wave equation (e.g., Hustedt et al., 2004; Operto et al., 2009; Liu et al., 2013; Tang et al., 2015). The frequency-domain scalar wave equation with PML boundary conditions (Bérenger, 1994) is written as follows:

$$\frac{\partial^2 P}{e_x^2 \partial x^2} + \frac{\partial^2 P}{e_x^2 \partial x^2} + \frac{\omega^2}{v^2} P = 0, \tag{18}$$

where

$$e_x = 1 + \frac{2\pi a_0 f_{peak}}{i\omega}\left(\frac{x_d}{L_{xpml}}\right)^2, \quad e_z = 1 + \frac{2\pi a_0 f_{peak}}{i\omega}\left(\frac{z_d}{L_{zpml}}\right)^2, \tag{19}$$

where i is an imaginary unit, e_x and e_z are the stretching functions in **X** and **Z** axis directions, respectively, x_d and z_d are the distances from the inner points of the PML boundaries along the **X** and **Z** axis directions, respectively, to the model boundary, L_{xpml} and L_{zpml} denote the widths of the PML boundaries along the **X** and **Z** axis directions, respectively, f_{peak} is the peak frequency of the source wavelet, and a_0 is a constant that can be determined by trial and error. The constant a_0 is assigned a value of 1.79 in this paper.

From eqs. (8), (10), and (18), the optimal 4th-order, 17-point DDM-based FD scheme with PML boundary conditions can be derived:

$$\begin{aligned}
&C_1 P_{m,n} + C_2\left(P_{m-1,n} + P_{m+1,n}\right) + C_3\left(P_{m,n-1} + P_{m,n+1}\right) + \\
&C_4\left(P_{m-2,n} + P_{m+2,n}\right) + C_5\left(P_{m,n-2} P_{m,n+2}\right) + \\
&C_6\left(P_{m-1,n-1} + P_{m+1,n-1} + P_{m-1,n+1} + P_{m+1,n+1}\right) + \\
&C_7\left(P_{m-2,n-2} + P_{m+2,n-2} + P_{m-2,n+2} + P_{m+2,n+2}\right) = 0,
\end{aligned} \tag{20}$$

where

$$
\begin{aligned}
&C_1 = \frac{-5a}{2e_x^2\Delta x^2} + \frac{-5a}{2e_z^2\Delta z^2} - 5(1-a)M + \frac{\omega_j^2}{v_{m,n}^2}b_1,\\
&C_2 = \frac{4}{3}\left(\frac{a}{e_x^2\Delta x^2} + (1-a)N\right) + \frac{\omega_j^2}{v_{m,n}^2}b_2,\quad C_3 = \frac{4}{3}\left(\frac{a}{e_z^2\Delta z^2} - (1-a)N\right) + \frac{\omega_j^2}{v_{m,n}^2}b_3,\\
&C_4 = \frac{-1}{12}\left(\frac{a}{e_x^2\Delta x^2} + (1-a)N\right) + \frac{\omega_j^2}{v_{m,n}^2}b_4,\quad C_5 = \frac{-1}{12}\left(\frac{a}{e_z^2\Delta z^2} - (1-a)N\right) + \frac{\omega_j^2}{v_{m,n}^2}b_5,\\
&C_6 = \frac{4(1-a)}{3}M + \frac{\omega_j^2}{v_{m,n}^2}b_6,\quad C_7 = \frac{-(1-a)}{12}M + \frac{\omega_j^2}{v_{m,n}^2}b_7,\\
&M = \frac{\Delta x^2 + \Delta z^2}{4\Delta x^2\Delta z^2},\quad N = \frac{\Delta z^2 - \Delta x^2}{2\Delta x^2\Delta z^2}.
\end{aligned}
\tag{21}
$$

NUMERICAL EXAMPLES

In this section, we present two homogeneous models to confirm the validity and accuracy of the optimal DDM 17-point scheme and one heterogeneous model to further demonstrate its adaptability to complex medium conditions.

Homogeneous model examples

To confirm the validity and accuracy of our DDM 17-point scheme, two simple 2D models are provided. First, we consider a whole homogeneous model with a velocity of 2500 m/s and grid dimensions of $Nx \times Nz = 201 \times 201$. In this case, an analytical solution is available to facilitate a comparison with the numerical solutions. A Ricker wavelet source is included in the forward modeling with a peak frequency of 25 Hz, and the waveform curve and amplitude spectrum are shown in Fig. 8. The maximum frequency used in the forward modeling is approximately 70 Hz on the premise of containing at least 99.9% of the effective spectrum energy. According to the sampling criterion of the DDM 17-point scheme (i.e., $G_{\min}$= 2.4), the maximum sampling interval is determined by $2500/70/2.4 \approx 14.88$ m. Thus, we design two sampling solutions:

$$\Delta x = \Delta z = 7 \text{ m},\ r = \Delta x/\Delta z = 1$$

and

$$\Delta x = 14 \text{ m}, \Delta z = 7 \text{ m},\ r = \Delta x/\Delta z = 2.$$

As shown in Fig. 7, the source is located at the center of the model. To observe the variations in the numerical dispersion with the propagation angle, five receivers (R_1, R_2, R_3, R_4, and R_5) are individually placed near the source. Specifically, receivers R_1 and R_5 are placed 50 grid units away from the source horizontally to the right and vertically downward at propagation

angles of 90° and 0°, respectively. When $\Delta x = \Delta z$, the receivers R_2, R_3 and R_4 represent propagation angles of 63.44°, 45° and 26.56°, respectively. Meanwhile, when $\Delta x = 2\Delta z$, the receivers R_2, R_3 and R_4 represent respective propagation angles of 76.96°, 63.44° and 45°.

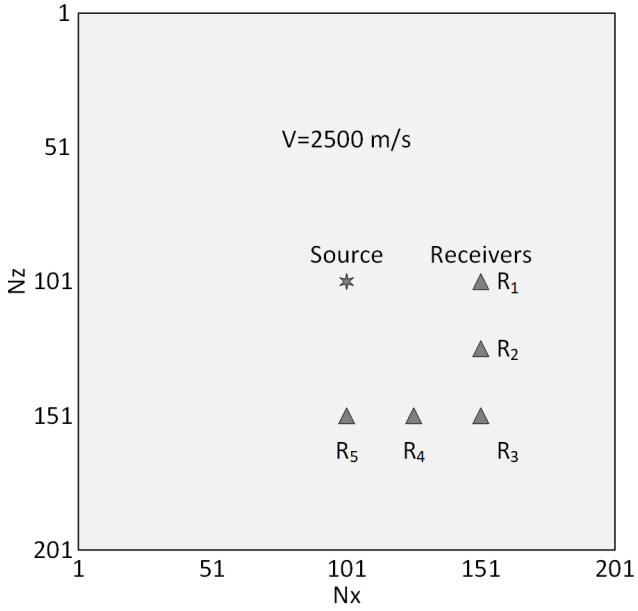

Fig. 7. Homogeneous velocity model.

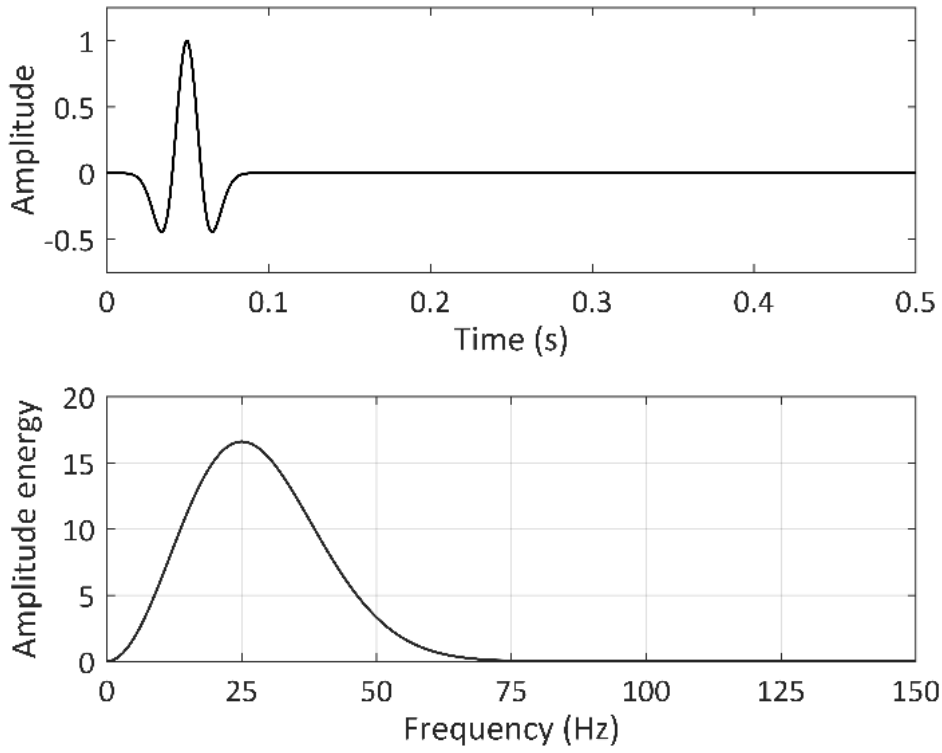

Fig. 8. Ricker wavelet with a peak frequency of 25 Hz and its amplitude spectrum.

We performed forward modeling on this homogeneous model using the conventional 4th-order, 9-point scheme, the ADM 17-point scheme and the proposed DDM 17-point scheme and compared the results with the analytical solutions. The thickness of the PML absorbing boundary is 50 units, and the recording time is 0.6 s, with an interval of 1 ms. The analytical solutions in a homogeneous medium are defined as follows (Alford et al., 1974):

$$P(\mathbf{x},t;\mathbf{s}) = \mathcal{F}^{-1}\left[-i\pi H_0^{(2)}\left(k|\mathbf{x}-\mathbf{s}|\right)\mathcal{F}\left(f(t)\right)\right], \tag{22}$$

where $\mathcal{F}$ and $\mathcal{F}^{-1}$ are the Fourier and inverse Fourier transformation operators, respectively, with respect to time, $f(t)$ is the time-domain Ricker wavelet, $H_0^{(2)}(x)$ is the second Hankel function of order zero, $k = \omega/v_0$ is the wavenumber, v_0 is the propagation velocity of the seismic wave, $|\mathbf{x}-\mathbf{s}|$ is the distance from the source to the receiver, $\mathbf{x}$ denotes the coordinates of the receiver, $\mathbf{s}$ denotes the coordinates of the source, and $P(\mathbf{x},t;\mathbf{s})$ represents the time-domain seismic wavefield excited by the source at position $\mathbf{s}$ and received by the receiver at position $\mathbf{x}$.

Fig. 9 shows the results (synthetic seismograms) recorded by the receivers R_1–R_5 for the two sampling solutions ($\Delta x = \Delta z$ and $\Delta x = 2\Delta z$) and the absolute error curves computed using eq. (22) with the conventional 4th-order, 9-point scheme, the ADM 17-point scheme and the proposed DDM 17-point scheme. Fig. 10 shows the mean absolute error (MAE) and standard deviation (SD) values calculated from the absolute error curves for the different receivers (R_1–R_5) shown in Fig. 9. In general, Fig. 9 provides the qualitative relationships between the forward modeling results and the analytical solutions while Fig. 10 provides the corresponding quantitative relationships. As shown in Fig. 9, the results from using the DDM 17-point scheme almost coincide with the analytical solutions with an MAE of approximately 0.01, thereby demonstrating that our proposed DDM 17-point scheme is correct. Moreover, the results for the case of $\Delta x = 2\Delta z$ prove that the proposed DDM 17-point scheme can be applied to different directional sampling intervals as well.

As shown in Fig. 9(a), the results obtained using the conventional 4th-order, 9-point scheme are in good accordance with the analytical solutions even though it is not optimized, because the sampling interval $\Delta x = \Delta z = 7$ m is smaller than its theoretical maximum interval $2500/70/5 \approx 7.14$ m, thereby satisfying the requirement for normalized phase velocity errors of $\pm 1\%$. The results obtained using the DDM 17-point scheme almost coincide with the analytical solutions, whereas the results acquired by employing the ADM 17-point scheme exhibit slight fluctuations, especially on either side of the main waveform. Therefore, the DDM 17-point scheme is overall more accurate than the ADM 17-point scheme. Remarkably, according to the MAE and SD values [Fig. 10(a)], the conventional 4th-order, 9-point scheme is the most accurate among the three FD schemes, and the DDM 17-point scheme is apparently superior to the ADM 17-point scheme when $\Delta x = \Delta z = 7$ m. In addition, the MAE and SE change patterns relative to the propagation angles [Fig. 10(a)] for the three FD schemes are symmetrical about R_3 (i.e., a 45° propagation angle), which is consistent with theoretical analysis.

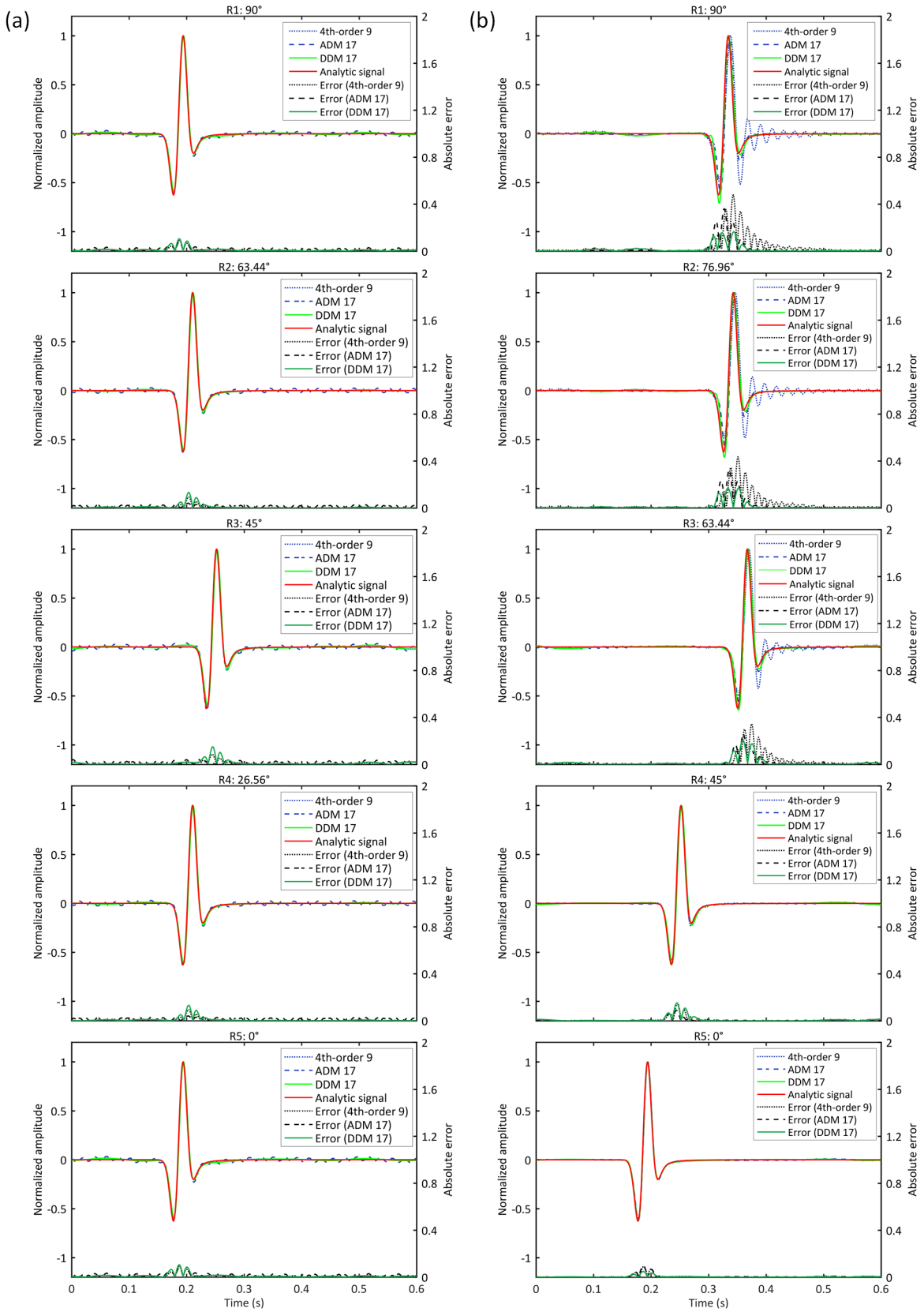

Fig. 9. Overlapping seismograms and absolute error curves for the different receivers (R_1–R_5) computed using the analytic method, the conventional 4th-order, 9-point scheme, the ADM-based 17-point scheme and the DDM-based 17-point scheme when $\Delta x = \Delta z = 7$ m (a) and $\Delta x = 14$ m, $\Delta z = 7$ m (b).

As shown in Fig. 9(b), the results of these three FD schemes gradually tend to draw close to the analytical solutions, indicating that their computational accuracies should increase with a decrease in the propagation angle in agreement with theoretical analysis. The results from the ADM and DDM 17-point schemes that have actual maximum grid intervals of 14 m, which are smaller than the theoretical maximum sampling interval (14.88 m), coincide well with the analytical solutions. The results received by R_5 (0° propagation angle) in the conventional 4th-order, 9-point scheme exhibit little numerical dispersion because the grid interval along the propagation direction is 7 m, which is less than the theoretical maximum sampling interval (7.14 m). However, relatively evident numerical dispersion is detected in the results for the other propagation angles due to grid intervals that are greater than 7.14 m. Furthermore, as shown in Fig. 10(b), the MAE and SD values of the DDM 17-point scheme for all of the propagation angles are smaller than those of the ADM 17-point scheme, revealing that the proposed DDM 17-point scheme possesses superior accuracy and more effectively suppresses dispersion in every propagation direction.

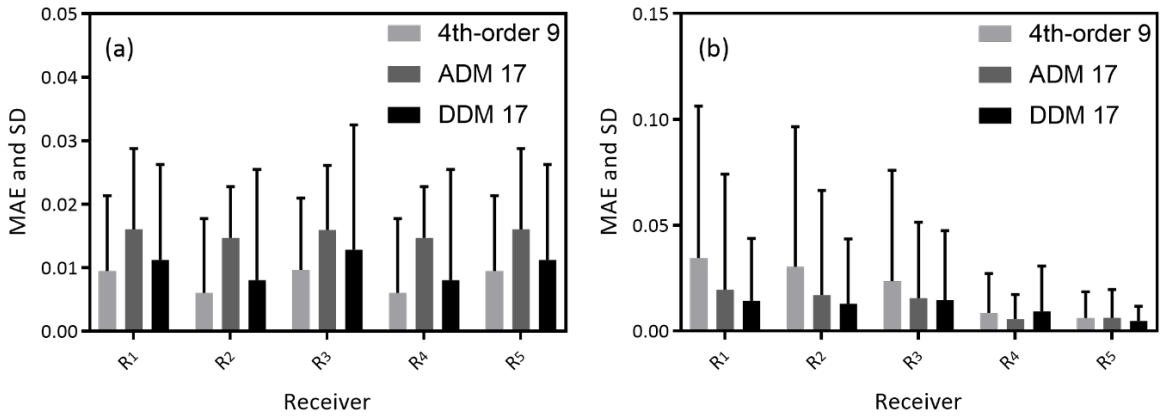

Fig. 10. Mean absolute error (MAE) and standard deviation (SD) values calculated from the absolute error curves for the different receivers (R_1–R_5) in Fig. 9 when $\Delta x = \Delta z = 7$ m (a) and $\Delta x = 14$ m, $\Delta z = 7$ m (b).

The second example is a horizontal two-layer model with velocities of 2000 m/s for the first layer and 3500 m/s for the second layer (Fig. 11). The horizontal and vertical grid dimensions are $Nx = 201$ and $Nz = 201$, respectively. The source, which is the same as that in the previous example, and the receivers are located at the top of the model (Fig. 11). For this model, two sampling solutions are employed ($\Delta x = \Delta z = 5$ m, $r = \Delta x/\Delta z = 1$ and $\Delta x = 11$ m, $\Delta z = 5.5$ m, $r = \Delta x/\Delta z = 2$) based on the theoretical maximum sampling interval ($2000/70/2.4 \approx 11.9$ m) to ensure the accuracy of the forward modeling. The recording times for the two sampling solutions are 0.65 s and 0.9 s, with an interval of 1 ms.

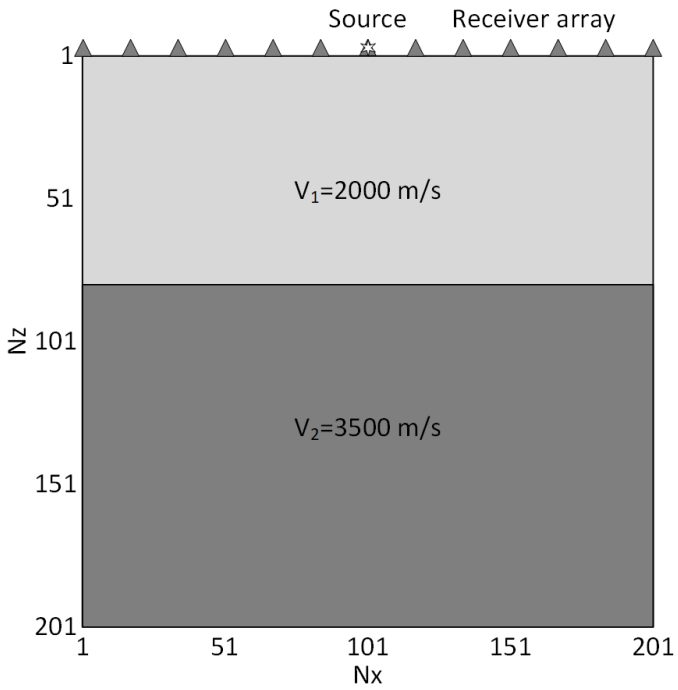

Fig. 11. Horizontally layered velocity model.

We performed forward modeling on this model to further confirm the validity of the DDM 17-point scheme compared with the conventional 4th-order, 9-point scheme and the time-domain FD method. The results from the time-domain method (with a 2nd-order accuracy in the time domain and a 12th-order accuracy in the spatial domain) are employed as a comparative standard because this method has the same accuracy as the frequency-domain 4th-order, 17-point FD scheme (Tang et al., 2015).

Fig. 12 and Fig. 13 show single-shot seismograms and wavefield snapshots, respectively, calculated using the abovementioned time-domain method and frequency-domain methods for the two sampling solutions. When $r = 1.0$, there is no numerical dispersion in the corresponding single-shot seismograms or wavefield snapshots since the grid interval ($\Delta x = \Delta z = 5$ m) is less than the theoretical maximum sampling interval ($2000/70/5 \approx 5.71$ m) for the conventional 4th-order, 9-point scheme. However, when $r = 2.0$, some apparent numerical dispersion appears within the results from the conventional 4th-order, 9-point scheme because the maximum grid interval (11 m) is greater than the theoretical maximum sampling interval [Fig. 12(b) and Fig. 13(b)]. Generally, the results from the proposed DDM 17-point scheme, which does not generate visible numerical dispersion, agree with those from the time-domain method. Moreover, as observed from the single-shot seismogram in Fig. 12(c) and the wavefield snapshot in Fig. 13(c), the boundary reflections are adequately suppressed by the configured PML absorbing boundaries, thereby demonstrating that the established FD scheme with PML absorbing boundaries [eq. (20)] is correct.

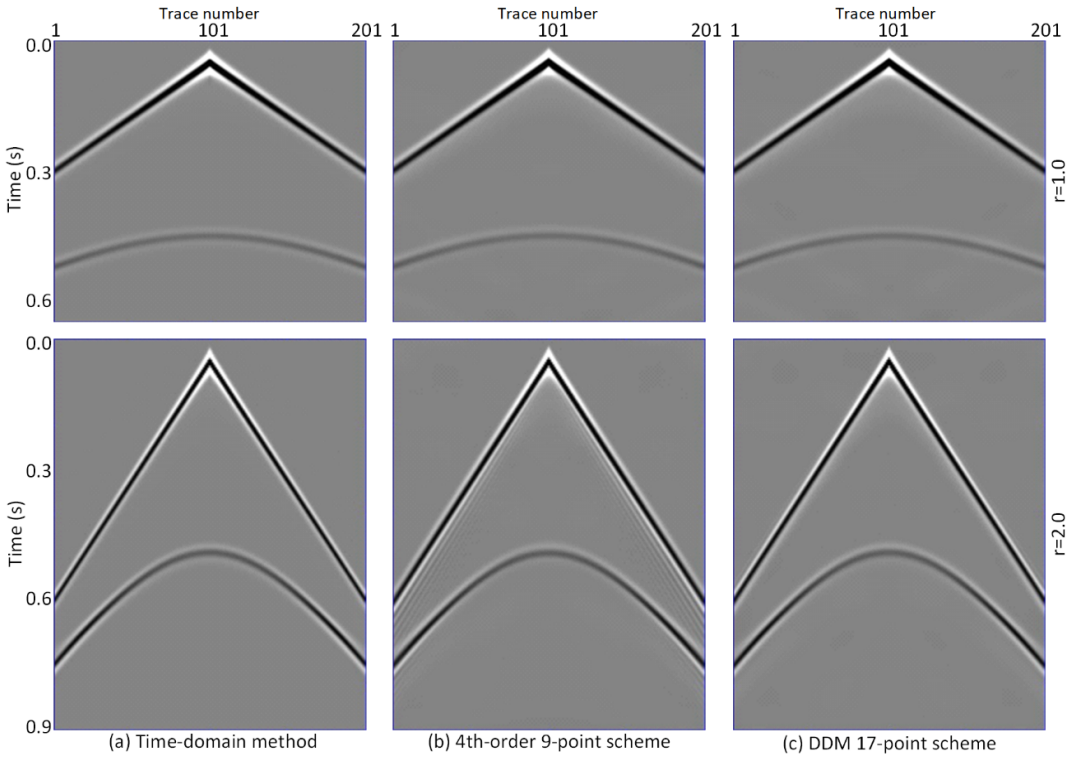

Fig. 12. Synthetic single-shot seismograms calculated using the time-domain method with a 2nd-order accuracy in time and a 12th-order accuracy in space (a), the 4th-order, 9-point scheme (b), and the DDM-based 17-point scheme (c) when $r = 1.0$ (the first row) and $r = 2.0$ (the second row).

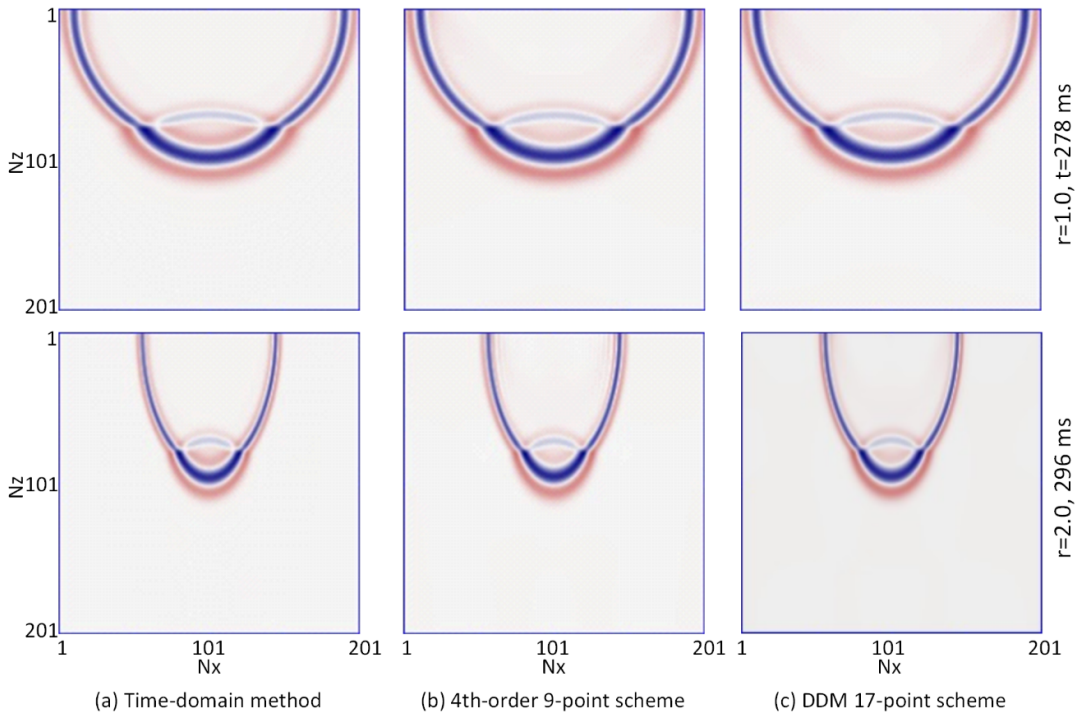

Fig. 13. Synthetic wavefield snapshots calculated using the time-domain method with a 2nd-order accuracy in time and a 12th-order accuracy in space (a), the 4th-order, 9-point scheme (b), and the DDM-based 17-point scheme (c) when $r = 1.0$, $t = 278$ ms (the first row) and $r = 2.0$, $t = 296$ ms (the second row).

Heterogeneous model examples

To demonstrate the adaptability of the DDM 17-point scheme to complex media, we applied a heterogeneous 2D salt model as shown in Fig. 14. The horizontal and vertical grid dimensions are $Nx = 201$ and $Nz = 191$, respectively, and the respective sampling intervals are $\Delta x = 12$ m and $\Delta z = 8$ m. For the ratio $r = \Delta x/\Delta z = 1.5$ of the directional sampling intervals, the corresponding optimization coefficients in Table 1 are a = 0.6992809, b_1 = 0.7854866, b_2 = 0.0837901, b_3 = 0.0600050, b_4 = -0.0183311, b_5 =-0.0068620, b_6 = -0.0024708, and b_7 = -0.0032019. A Ricker wavelet is employed as the source, with a peak frequency of 15 Hz at the position (x = 1200 m, z = 0 m), and the recording time is 1.4 s, with an interval of 1 ms. The receivers are uniformly placed on either side of the source point, with an interval of 12 m.

Fig. 15 and Fig. 16 show the single-shot seismograms and wavefield snapshots (t = 535 ms) obtained using the proposed DDM 17-point scheme and the time-domain method, respectively. Both the seismogram [Fig. 15(b)] and the wavefield snapshot [Fig. 16(b)] obtained using the DDM 17-point scheme not only lack numerical dispersion but also agree well with the results using the time-domain method [Fig. 15(a) and Fig. 16(a)] with respect to their dynamic and kinematic characteristics. Therefore, we conclude that the DDM 17-point FD scheme has good adaptability to not only simple media models but also complex media models.

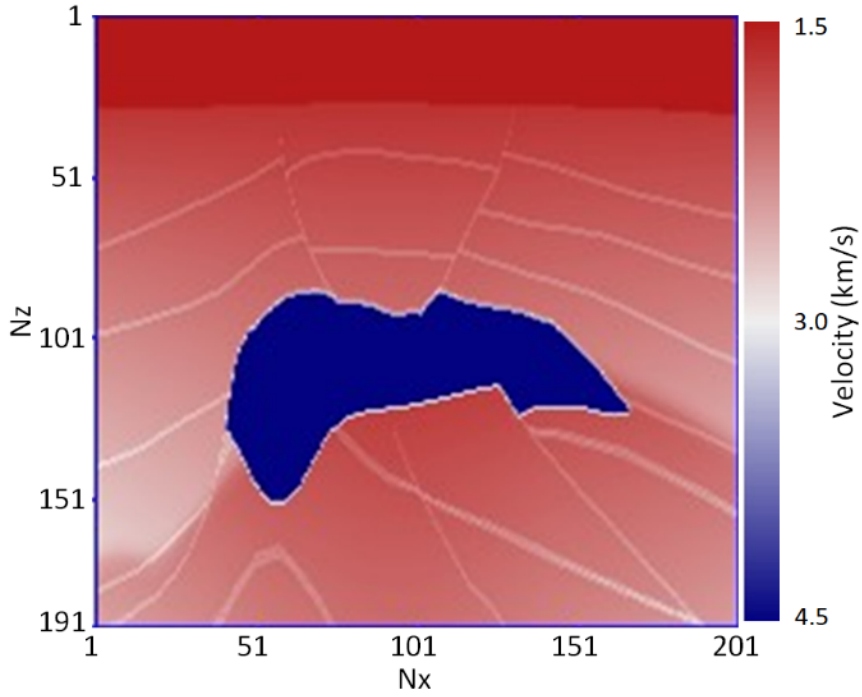

Fig. 14. Heterogeneous salt model.

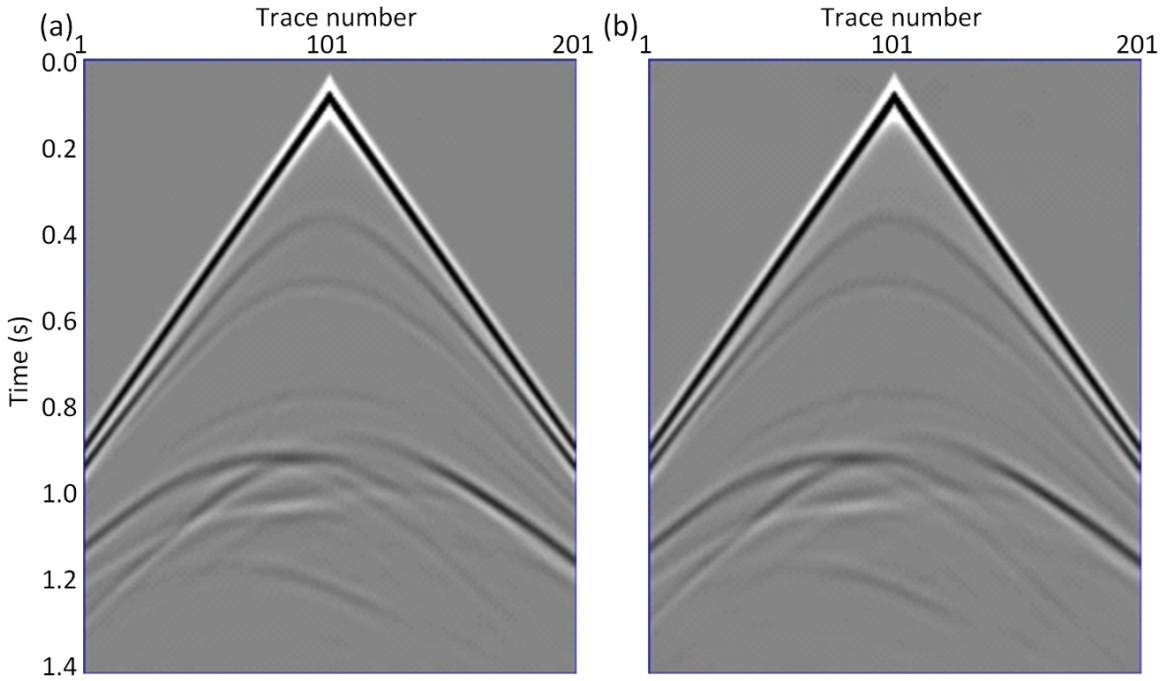

Fig. 15. Synthetic single-shot seismograms calculated using the time-domain method with a 2nd-order accuracy in time and a 12th-order accuracy in space (a) and the DDM-based 17-point scheme (b).

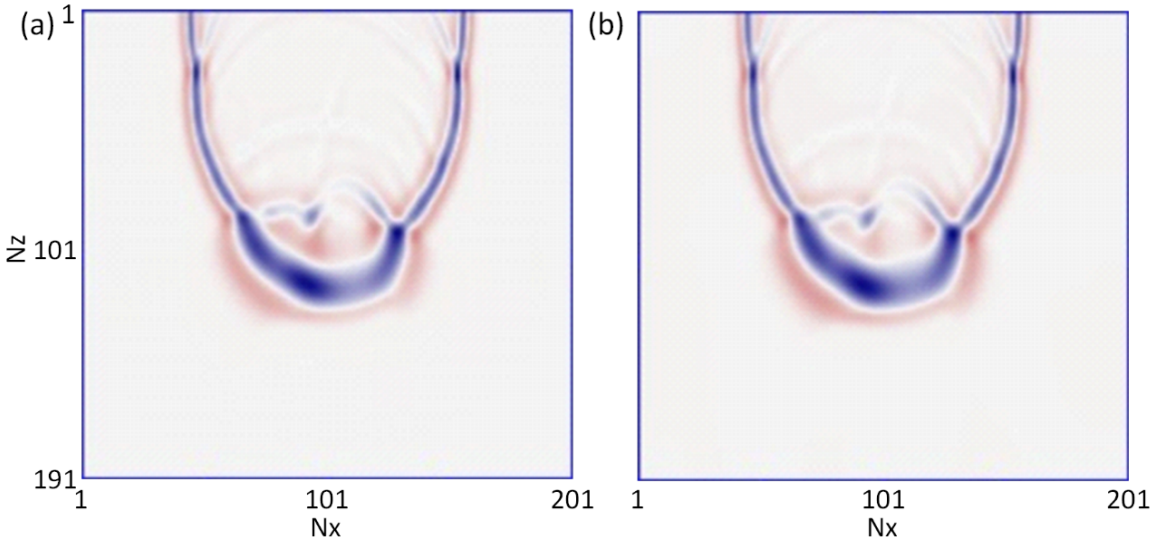

Fig. 16. Synthetic wavefield snapshots (t = 535 ms) calculated using the time-domain method with a 2nd-order accuracy in time and a 12th-order accuracy in space (a) and the DDM-based 17-point scheme (b).

CONCLUSIONS

We have proposed a novel frequency-domain 17-point FD scheme based on the DDM for the 2D scalar wave equation. This new scheme not only extends the application scope of the conventional rotated optimal 17-point FD scheme by removing the requirement for equal directional

sampling intervals but also retains the geometrical properties of the rotating coordinate system. Theoretical analyses indicate that the optimized DDM-based 17-point scheme can reduce the number of grids per the shortest wavelength from 2.56 to less than 2.4 for maximum phase velocity errors of 1% and can both improve the computational efficiency and decrease the memory requirements while maintaining the same accuracy. Besides, the classical 4th-order, 9-point scheme and the rotated optimal 17-point scheme are two special cases of the DDM-based 17-point scheme. The validity and accuracy of the new optimal DDM-based 17-point scheme are confirmed through the comparison with the analytical solutions of homogeneous examples. In addition, the new scheme is superior to the ADM 17-point scheme and possesses a higher accuracy and is more capable of suppressing numerical dispersion resulting from the geometrical properties of the rotating coordinate system. A heterogeneous example further demonstrates the adaptability of the proposed method to complex media. In general, the new scheme enhances the application scope of the 17-point FD scheme and provides an effective and flexible forward modeling method for high-precision FWI in the frequency domain.

ACKNOWLEDGMENTS

We would like to thank the editors in charge and the anonymous reviewers for their thoughtful reviews and valuable comments that helped to improve the quality of this paper. We also thank Jia Tang for providing useful suggestions. This research was supported by the National Natural Science Foundation of China (Grant No. 61775030, 61571096, 41301460, and 41274127).

REFERENCES

Alford, R.M., Kelly, K.R. and Boore, D.M., 1974. Accuracy of finite-difference modeling of the acoustic wave equation. Geophysics, 39: 834-842.

Bérenger, J.P., 1994. A perfectly matched layer for the absorption of electromagnetic waves. J. Comput. Phys., 114: 185-200.

Brossier, R., Operto, S. and Virieux, J., 2009. Seismic imaging of complex onshore structures by 2D elastic frequency-domain full-waveform inversion. Geophysics, 74(6): WCC105-118.

Cao, S.H. and Chen, J.B., 2012. A 17-point scheme and its numerical implementation for high-accuracy modeling of frequency-domain acoustic equation. Chin. J. Geophys. (in Chinese), 55: 3440-3449.

Chen, J.B., 2013. A generalized optimal 9-point scheme for frequency-domain scalar wave equation. J. Appl. Geophys., 92: 1-7. doi: 10.1016/j.jappgeo.2013.02.008.

Chen, J.B., 2012. An average-derivative optimal scheme for frequency-domain scalar wave equation. Geophysics, 77(6): T201-T210.

Chen, J.B., 2008. Variational integrators and the finite element method. Appl. Math. Comput., 196: 941-958.

Fan, N., Zhao, L.-F. and Xie, X.-B., 2017. A general optimal method for a 2D frequency-domain finite-difference solution of scalar wave equation. Geophysics, 82(3): T121-T132.

Gauthier, O., Virieux, J. and Tarantola, A., 1986. Two-dimensional nonlinear inversion of seismic waveforms: Numerical results. Geophysics, 51: 1387–1403.

Ha, W. and Shin, C., 2012. Laplace-domain full-waveform inversion of seismic data lacking low-frequency information. Geophysics, 77(5): R199–R206.

Ha, W. and Shin, C., 2013. Why do Laplace-domain waveform inversions yield long-wavelength results? Geophysics, 78(4): R167-R173.

Hustedt, B., Operto, S. and Virieux, J., 2004. Mixed-grid and staggered-grid finite-difference methods for frequency-domain acoustic wave modelling. Geophys. J. Internat., 157: 1269–1296.

Jo, C.H., Suh, J.H. and Shin, C.S., 1996. An optimal 9-point, finite-difference, frequency-space, 2-D scalar wave extrapolator. Geophysics, 61: 529-537.

Kamei, R., Pratt, R.G. and Tsuji, T., 2015. Misfit functionals in Laplace-Fourier domain waveform inversion, with application to wide□angle ocean bottom seismograph data. Geophys. Prosp., 62: 1054-1074.

Lee, D., Cha, Y.H. and Shin, C., 2008. The direct-removal method of waveform inversion in the Laplace inversion for deep-sea environments. Expanded Abstr., 78th Ann. Internat. SEG Mtg., Las Vegas: 1981-1985.

Liu, L., Liu, H. and Liu, H., 2013. Optimal 15-point finite difference forward modeling in frequency-space domain. Chin. J. Geophys. (in Chinese), 56: 644-652.

Lysmer, J. and Drake, L.A., 1972. A finite element method for seismology. Methods Comput. Phys. Adv. Res. Appl., 11: 181-216.

Marfurt, K.J., 1984. Accuracy of finite-difference and finite-element modeling of the scalar and elastic wave equations. Geophysics, 49: 533-549.

Min, D.-J., Shin, C., Pratt, R.G. and Yoo, H.S., 2003. Weighted-averaging finite-element method for 2D elastic wave equations in the frequency domain. Bull. Seismol. Soc. Am., 93: 904-921.

Operto, S., Virieux, J., Amestoy, P.R., Excellent, J.L., Giraud, L. and Ali, H.B.H., 2007. 3D finite-difference frequency-domain modeling of visco-acoustic wave propagation using a massively parallel direct solver: A feasibility study. Geophysics, 72(5), SM195-SM211.

Operto, S., Virieux, J., Ribodetti, A. and Anderson, J.E., 2009. Finite-difference frequency-domain modeling of viscoacoustic wave propagation in 2D tilted transversely isotropic (TTI) media. Geophysics, 74(5), T75–T95.

Pratt, R.G., 1990. Frequency-domain elastic wave modeling by finite differences: A tool for crosshole seismic imaging. Geophysics, 55: 626-632.

Pratt, R.G., 1999. Seismic waveform inversion in the frequency domain; Part 1, Theory and verification in a physical scale model. Geophysics, 64: 888-901.

Pratt, R.G., Shin, C. and Hick, G.J., 1998. Gauss-Newton and full Newton methods in frequency-space seismic waveform inversion. Geophys. J. Internat., 133: 341-362.

Pratt, R.G. and Worthington, M.H., 1990a. Inverse theory applied to multi-source cross-hole tomography. Part 1: acoustic wave-equation method. Geophys. Prosp., 38: 287-310.

Pratt, R.G. and Worthington, M.H., 1990b. Inverse theory applied to multi-source cross-hole tomography. Part 2: elastic wave-equation method. Geophys. Prosp., 38: 311-329.

Pyun, S., Shin, C., Lee, H. and Yang, D., 2008. 3D elastic full waveform inversion in the Laplace domain. Expand. Abstr., 78th Ann. Internat. SEG Mtg., Las Vegas: 1976-1980.

Saenger, E.H., Gold, N. and Shapiro, S.A., 2000. Modeling the propagation of elastic waves using a modified finite-difference grid. Wave Motion, 31: 77-92.

Shin, C. and Cha, Y.H., 2009. Waveform inversion in the Laplace-Fourier domain. Geophys. J. Internat., 177: 1067-1079.

Shin, C. and Cha, Y.H., 2008. Waveform inversion in the Laplace domain. Geophys. J. Internat., 173: 922-931.

Shin, C., Koo, N.H., Cha, H.Y. and Park, K.P., 2010. Sequentially ordered single-frequency 2-D acoustic waveform inversion in the Laplace-Fourier domain. Geophys. J. Internat., 181: 935-950.

Shin, C. and Sohn, H., 1998. A frequency-space 2-D scalar wave extrapolator using extended 25-point finite-difference operator. Geophysics, 63: 289-296.

Shin, J., Kim, Y., Shin, C. and Calandra, H., 2013. Laplace-domain full waveform inversion using irregular finite elements for complex foothill environments. J. Appl. Geophys., 96(9): 67–76.

Štekl, I. and Pratt, R.G., 1998. Accurate viscoelastic modeling by frequency-domain finite-differences using rotated operators. Geophysics, 63: 1779-1794.

Tang, X. De, Liu, H., Zhang, H., Liu, L. and Wang, Z.Y., 2015. An adaptable 17-point scheme for high-accuracy frequency-domain acoustic wave modeling in 2D constant density media. Geophysics, 80(6), T211-T221.

Tarantola, A., 1984. Inversion of seismic reflection data in acoustic approximation. Geophysics, 49: 1259-1266.

Virieux, J. and Operto, S., 2009. An overview of full-waveform inversion in exploration geophysics. Geophysics, 74(6): WCC1-WCC26.

Yang, Q., Hu, G. and Wang, L., 2014. Research status and development trend of full waveform inversion. Geophys. Prosp. Pet., 53: 77-83.

Zhang, H., Liu, H., Liu, L., Jin, W.J. and Shi, X.D., 2014. Frequency domain acoustic equation high-order modeling based on an average-derivative method. Chin. J. Geophys. (in Chinese), 57: 1599-1612.

APPENDIX

FINITE-DIFFERENCE DISCRETIZATION FOR THE LAPLACIAN OPERATOR (SECOND-ORDER SPATIAL DERIVATIVE) OF THE 45° ROTATING COORDINATE SYSTEM

The following derivation process is provided to prove that the finite-difference approximation of the Laplacian in a 45° rotating coordinate system can be applied only to equal directional sampling intervals (i.e., a square sampling grid).

The finite-difference approximation of the Laplacian in a 45° rotating coordinate system is given as (Cao and Chen, 2012)

$$\frac{\partial^2 P}{\partial x^2}\Big|_{m,n} + \frac{\partial^2 P}{\partial z^2}\Big|_{m,n} = \frac{-\frac{1}{12}\left(P_{m-2,n-2} + P_{m+2,n+2}\right) + \frac{4}{3}\left(P_{m-1,n-1} + P_{m+1,n+1}\right) - \frac{5}{2}P_{m,n}}{\Delta x^2 + \Delta z^2} + \frac{-\frac{1}{12}\left(P_{m+2,n-2} + P_{m-2,n+2}\right) + \frac{4}{3}\left(P_{m+1,n-1} + P_{m-1,n+1}\right) - \frac{5}{2}P_{m,n}}{\Delta x^2 + \Delta z^2}. \quad \text{(A-1)}$$

Performing a second-order Taylor expansion of the terms ($P_{m-2,n-2}$, $P_{m+2,n-2}$, $P_{m+2,n+2}$, $P_{m-2,n+2}$, $P_{m-1,n-1}$, $P_{m+1,n-1}$, $P_{m+1,n+1}$ and $P_{m-1,n+1}$) on the right-hand side of eq. (A-1), we can obtain

$$P_{m-2,n-2} = P_{m,n} + \left(\frac{\partial P}{\partial x}\Big|_{m,n} (-2\Delta x) + \frac{\partial P}{\partial z}\Big|_{m,n} (-2\Delta z) \right) +$$
$$\frac{1}{2}\left(\frac{\partial^2 P}{\partial x^2}\Big|_{m,n} (-2\Delta x)^2 + \frac{\partial^2 P}{\partial z^2}\Big|_{m,n} (-2\Delta z)^2 + \frac{\partial^2 P}{\partial x \partial z}\Big|_{m,n} 4\Delta x \Delta z \right) + o\left(\Delta x^2, \Delta z^2\right)$$
$$P_{m+2,n+2} = P_{m,n} + \left(\frac{\partial P}{\partial x}\Big|_{m,n} (2\Delta x) + \frac{\partial P}{\partial z}\Big|_{m,n} (2\Delta z) \right) +$$
$$\frac{1}{2}\left(\frac{\partial^2 P}{\partial x^2}\Big|_{m,n} (2\Delta x)^2 + \frac{\partial^2 P}{\partial z^2}\Big|_{m,n} (2\Delta z)^2 + \frac{\partial^2 P}{\partial x \partial z}\Big|_{m,n} 4\Delta x \Delta z \right) + o\left(\Delta x^2, \Delta z^2\right)$$
$$P_{m-2,n+2} = P_{m,n} + \left(\frac{\partial P}{\partial x}\Big|_{m,n} (-2\Delta x) + \frac{\partial P}{\partial z}\Big|_{m,n} (2\Delta z) \right) +$$
$$\frac{1}{2}\left(\frac{\partial^2 P}{\partial x^2}\Big|_{m,n} (-2\Delta x)^2 + \frac{\partial^2 P}{\partial z^2}\Big|_{m,n} (2\Delta z)^2 - \frac{\partial^2 P}{\partial x \partial z}\Big|_{m,n} 4\Delta x \Delta z \right) + o\left(\Delta x^2, \Delta z^2\right)$$
$$P_{m+2,n-2} = P_{m,n} + \left(\frac{\partial P}{\partial x}\Big|_{m,n} (2\Delta x) + \frac{\partial P}{\partial z}\Big|_{m,n} (-2\Delta z) \right) +$$
$$\frac{1}{2}\left(\frac{\partial^2 P}{\partial x^2}\Big|_{m,n} (2\Delta x)^2 + \frac{\partial^2 P}{\partial z^2}\Big|_{m,n} (-2\Delta z)^2 - \frac{\partial^2 P}{\partial x \partial z}\Big|_{m,n} 4\Delta x \Delta z \right) + o\left(\Delta x^2, \Delta z^2\right), \qquad \text{(A-2)}$$

and

$$P_{m-1,n-1} = P_{m,n} + \left(\frac{\partial P}{\partial x}\Big|_{m,n} (-\Delta x) + \frac{\partial P}{\partial z}\Big|_{m,n} (-\Delta z) \right) +$$
$$\frac{1}{2}\left(\frac{\partial^2 P}{\partial x^2}\Big|_{m,n} (-\Delta x)^2 + \frac{\partial^2 P}{\partial z^2}\Big|_{m,n} (-\Delta z)^2 + \frac{\partial^2 P}{\partial x \partial z}\Big|_{m,n} \Delta x \Delta z \right) + o\left(\Delta x^2, \Delta z^2\right)$$
$$P_{m+1,n+1} = P_{m,n} + \left(\frac{\partial P}{\partial x}\Big|_{m,n} (\Delta x) + \frac{\partial P}{\partial z}\Big|_{m,n} (\Delta z) \right) +$$
$$\frac{1}{2}\left(\frac{\partial^2 P}{\partial x^2}\Big|_{m,n} (\Delta x)^2 + \frac{\partial^2 P}{\partial z^2}\Big|_{m,n} (\Delta z)^2 + \frac{\partial^2 P}{\partial x \partial z}\Big|_{m,n} \Delta x \Delta z \right) + o\left(\Delta x^2, \Delta z^2\right)$$
$$P_{m-1,n+1} = P_{m,n} + \left(\frac{\partial P}{\partial x}\Big|_{m,n} (-\Delta x) + \frac{\partial P}{\partial z}\Big|_{m,n} (\Delta z) \right) +$$
$$\frac{1}{2}\left(\frac{\partial^2 P}{\partial x^2}\Big|_{m,n} (-\Delta x)^2 + \frac{\partial^2 P}{\partial z^2}\Big|_{m,n} (\Delta z)^2 - \frac{\partial^2 P}{\partial x \partial z}\Big|_{m,n} \Delta x \Delta z \right) + o\left(\Delta x^2, \Delta z^2\right)$$
$$P_{m+1,n-1} = P_{m,n} + \left(\frac{\partial P}{\partial x}\Big|_{m,n} (\Delta x) + \frac{\partial P}{\partial z}\Big|_{m,n} (-\Delta z) \right) +$$
$$\frac{1}{2}\left(\frac{\partial^2 P}{\partial x^2}\Big|_{m,n} (\Delta x)^2 + \frac{\partial^2 P}{\partial z^2}\Big|_{m,n} (-\Delta z)^2 - \frac{\partial^2 P}{\partial x \partial z}\Big|_{m,n} \Delta x \Delta z \right) + o\left(\Delta x^2, \Delta z^2\right). \qquad \text{(A-3)}$$

Then

$$-\frac{1}{12}\left(P_{m-2,n-2}+P_{m+2,n+2}+P_{m-2,n+2}+P_{m+2,n-2}\right)=-\frac{1}{3}\left(P_{m,n}+2\Delta x^2\frac{\partial^2 P}{\partial x^2}\Big|_{m,n}+2\Delta z^2\frac{\partial^2 P}{\partial z^2}\Big|_{m,n}\right)+o\left(\Delta x^2,\Delta z^2\right)$$

$$\frac{4}{3}\left(P_{m-1,n-1}+P_{m+1,n+1}+P_{m-1,n+1}+P_{m+1,n-1}\right)=\frac{4}{3}\left(4P_{m,n}+2\Delta x^2\frac{\partial^2 P}{\partial x^2}\Big|_{m,n}+2\Delta z^2\frac{\partial^2 P}{\partial z^2}\Big|_{m,n}\right)+o\left(\Delta x^2,\Delta z^2\right).$$

(A-4)

Substituting eq. (A-4) into eq. (A-1), we can obtain

$$\frac{\partial^2 P}{\partial x^2}\Big|_{m,n}+\frac{\partial^2 P}{\partial z^2}\Big|_{m,n}=\frac{2\Delta x^2}{\Delta x^2+\Delta z^2}\frac{\partial^2 P}{\partial x^2}\Big|_{m,n}+\frac{2\Delta z^2}{\Delta x^2+\Delta z^2}\frac{\partial^2 P}{\partial z^2}\Big|_{m,n}+o\left(\Delta x^2,\Delta z^2\right). \qquad \text{(A-5)}$$

Eq. (A-5) is true only when $\Delta x = \Delta z$. That is, the right-hand side of eq. (A-1) is not an approximation for the Laplacian $\frac{\partial^2 P}{\partial x^2}+\frac{\partial^2 P}{\partial z^2}$ at point (m,n) because $\frac{2\Delta x^2}{\Delta x^2+\Delta z^2} \neq \frac{2\Delta z^2}{\Delta x^2+\Delta z^2}$.